

A Universal Metric of Dataset Similarity for Cross-silo Federated Learning

Ahmed Elhussein

*Department of Biomedical Informatics, Columbia University
New York Genome Center*

AE2722@CUMC.COLUMBIA.EDU

Gamze Gürsoy

*Department of Biomedical Informatics, Columbia University
New York Genome Center*

GAMZE.GURSOY@COLUMBIA.EDU

Department of Computer Science, Columbia University

Abstract

Federated Learning is increasingly used in domains such as healthcare to facilitate collaborative model training without data-sharing. However, datasets located in different sites are often non-identically distributed, leading to degradation of model performance in FL. Most existing methods for assessing these distribution shifts are limited by being dataset or task-specific. Moreover, these metrics can only be calculated by exchanging data, a practice restricted in many FL scenarios. To address these challenges, we propose a novel metric for assessing dataset similarity. Our metric exhibits several desirable properties for FL: it is dataset-agnostic, is calculated in a privacy-preserving manner, and is computationally efficient, requiring no model training. In this paper, we first establish a theoretical connection between our metric and training dynamics in FL. Next, we extensively evaluate our metric on a range of datasets including synthetic, benchmark, and medical imaging datasets. We demonstrate that our metric shows a robust and interpretable relationship with model performance and can be calculated in privacy-preserving manner. As the first federated dataset similarity metric, we believe this metric can better facilitate successful collaborations between sites.

Keywords: federated learning, optimal transport, dataset similarity, privacy-preservation

1 Introduction

Federated Learning (FL) is a distributed learning framework that enables collaborative model training without data-sharing. This approach is valuable in sectors such as healthcare and insurance where institutional and/or corporate policies and regulations might prohibit data-sharing (Huang et al., 2021). In these *cross-silo* settings, FL increases sample sizes and improves model performance (Zhao et al., 2020). A common approach to creating a global model in FL is via the Federated Averaging (FedAvg) algorithm, where a server averages local updates from each client to create a global model. However, when data is collected from different sites, it is often non-identically independently distributed (non-IID) leading to weight divergence in client updates, degrading model performance (Hsieh et al., 2020; Li et al., 2022). This can discourage future cooperation in settings like healthcare, where increasing sample size might be critical (Tu et al., 2022). While personalized FL methods

aim to tackle issues with non-IID data, they do not consistently surpass the performance of the standard Federated Averaging (FedAvg) approach. Furthermore, their increased complexity often necessitates careful hyperparameter tuning and larger sample sizes.

Assessing dataset similarity can help to determine appropriateness of FL and guide the selection of algorithms for personalized approaches when necessary. However, in a federated context, diagnosing when and how datasets differ is challenging due to the *site-specific* nature of data generation processes, which are heterogeneous and often unknown (Zhang et al., 2022; Hripcsak and Albers, 2013). When differences among a set of clients are substantial, they can lead to significant distribution shifts, causing performance of FL to fall below that of local training (Li et al., 2022). For example, an international consortium of hospitals with sufficiently different diagnostic criteria may not benefit from training a shared diagnosis model (Futoma et al., 2020). While this issue can be avoided by grouping subsets of clients with similar datasets using cluster-based FL or by implementing personalized FL algorithms, selecting the most suitable approach requires a thorough understanding of dataset similarity across these hospitals.

Current methods for evaluating dataset similarity fall under three categories: measuring distance between datasets, learning a mapping function between datasets, and estimating parameter sensitivity of the models (Alvarez-Melis and Fusi, 2020; Courty et al., 2017; Damodaran et al., 2018; Pándy et al., 2022; Cortes and Mohri, 2011; Achille et al., 2019). Despite their success in domains like transfer learning, these methods are not suitable for FL. First, most methods require access to individual data points (sample-level data) from all datasets, which may not be possible in cross-silo settings (Butler, 2007). Second, these methods are often dataset- or task-specific, limiting their generalizability. This arises because the similarity scores generated by these methods are unbounded, hence depending on dataset dimension and scale among other factors. Consequently, interpreting whether a score indicates similar or dissimilar datasets requires understanding specific characteristics of the dataset or task. Third, they primarily focus on unlabeled data and cannot be used for supervised learning, which is a more prevalent use-case in FL. Finally, methods that learn a mapping function or estimate parameter sensitivity rely on training a specific model for the task, requiring large sample sizes. Here we propose that an ideal dataset similarity metric for cross-silo FL should be *privacy-preserving, adaptable across diverse datasets and tasks, capable of integrating label information, and effective without the need for large datasets*.

We propose a novel bounded metric designed to estimate dataset similarity, determine the effectiveness of FL, and inform training decisions. Our metric addresses specific challenges in cross-silo FL, particularly the restricted access to data across different sites and the limited sample sizes available at individual sites. Specifically, it (1) provides a universal measure that is not dataset specific and is label-aware; (2) is privacy-preserving; (3) has low sample complexity. Our metric leverages optimal transport (OT) to compute a bounded score between every pair of data points, taking into account both feature and label distributions. We achieve this by replacing the Euclidean-distance cost function in OT with a hybrid cosine similarity-Hellinger distance cost function. We provide a theoretical justification explaining how this metric effectively captures FL weight divergence, a measure that quantifies the extent to which model updates differ due to heterogeneous data distributions. Further, we show that the hybrid cosine similarity-Hellinger distance cost function is a valid OT cost function. We then demonstrate that our metric outperforms original Wasserstein distance in

predicting training performance and supporting hyperparameter selection across a range of datasets, including real-world medical imaging datasets. Our approach has the potential to avoid inefficient training on non-IID data.

2 Related Work

Alvarez-Melis and Fusi (2020) proposed an OT based approach that incorporated label-awareness and eliminated the need for training while calculating dataset similarity. Their method leveraged a combination of Euclidean distance for label distributions and Wasserstein distance for feature distributions to quantify the dissimilarity between data points. They demonstrated a correlation between dataset distance and transfer learning performance. However, their measure is unbounded and sensitive to the scale of the data points.

Label-aware methods that require model training include methods that measure joint label-feature distributions (*e.g.*, JDOT by Courty et al. (2017), DeepJDOT by Damodaran et al. (2018)) and methods that transform datasets via Wasserstein gradient flows (Alvarez-Melis and Fusi, 2021). However, these methods require model training. Further, these methods require access to the data to estimate the underlying distributions, which is not possible in cross-silo settings.

Pándy et al. (2022) developed a bounded metric using Bhattacharyya distance between dataset embeddings. However, this metric is label-unaware and requires training. Moreover, sharing of dataset embeddings across sites might not be allowed in cross-silo settings.

Discrepancy measures and parameter sensitivity have also been used to quantify similarity between datasets in domain adaptation and meta-learning, respectively (Cortes and Mohri, 2011; Achille et al., 2019; Ben-David et al., 2006; Mansour et al., 2009; Achille et al., 2018; Liang et al., 2019; Li, 2006). Discrepancy measures depend on learning a function that maps features from the source to the target domain. Parameter sensitivity based methods use information-theoretic measures to quantify model sensitivity to specific parameters. These methods work well in providing generalization bounds. However, they require large sample size and careful model selection.

3 Background

We cover preliminaries related to the problem and our proposed solution. Note, for brevity, we leave privacy preliminaries related to secure Multi Party Computation (MPC) and Differential Privacy (DP) to Appendix A.

3.1 Federated Learning

In FL, a server and client network iteratively train a model. First, the server distributes model parameters; clients then train the model and send model updates back to the server; finally the server aggregates the updates, typically via weighted average in FedAvg. However, when clients optimize a local model exclusively on their data, their updates can diverge from the global model, if their data is non-IID. Zhao et al. (2018) defined weight divergence as

$$\frac{\|w^{Global} - w^{Local}\|}{\|w^{Local}\|}. \quad (1)$$

3.2 Optimal Transport

OT is a framework that quantifies the dissimilarity between probability distributions by defining a cost function between distributions and then identifying the optimal transportation map that minimizes this cost (Villani et al., 2009). The Kantorovich (1960) formulation of OT between two distributions X and Y is

$$OT(X, Y) := \min_{\pi \in \Pi(X, Y)} \int_{\mathcal{X} \times \mathcal{Y}} c(x, y) d\pi(x, y) \quad (2)$$

where $c(x, y)$ is the cost function between two points and $\Pi(X, Y)$ is the couplings over the product space $\mathcal{X} \times \mathcal{Y}$. When $c(x, y)$ is defined using euclidean distance, OT cost is called the p-Wasserstein distance. For scenarios involving finite samples, there exists an OT formulation that utilizes discrete samples. Here, the pairwise cost between data points is represented as an $n \times m$ matrix where $C_{i,j} = c(x_i, y_j)$. In this case, Equation 2 has a cubic complexity and is replaced by an entropy-regularized Sinkhorn formulation (Cuturi, 2013)

$$\min_{\pi \in \Pi(X, Y)} \int_{\mathcal{X} \times \mathcal{Y}} c(x, y) d\pi(x, y) + \epsilon H(\pi | X \otimes Y) \quad (3)$$

where $H(\pi | X \otimes Y)$ is the relative entropy.

4 Proposed Framework

We introduce the problem of assessing dataset similarity in FL before describing our metric.

4.1 Problem setup

In supervised learning a dataset consists of feature-label pairs (x, y) , where $x \in \mathcal{X}$ and $y \in \mathcal{Y}$ and \mathcal{X} and \mathcal{Y} denote the feature space and label set, respectively. We use z to denote the (x, y) pair. Let us assume two distinct datasets, \mathcal{D}_1 and \mathcal{D}_2 where the feature vectors are denoted as x_i and x_j and the corresponding labels are represented as y_i^c and $y_j^{c'}$, respectively. Here i and j refer to indices of the specific data points and c and c' refer to label *classes*. Our goal is to calculate the OT score between two datasets in a federated setting. Specifically, the metric should be calculable in privacy preserving manner, utilize a dataset agnostic cost function, and require few samples.

4.2 Dataset Similarity Metric

Our approach is detailed in Algorithm 1. Briefly, we replace Euclidean distance with a combination of cosine similarity and Hellinger distance as our OT cost function. For feature cost, we compute pairwise cosine similarities between samples from \mathcal{D}_1 and \mathcal{D}_2 . For label cost, we first model labels as distributions over their features, following the approach of Alvarez-Melis and Fusi (2020). We then calculate the Hellinger distance between each pair of label distributions. To construct the final cost matrix, we sum the respective feature and label costs for every pair of samples. As both feature and label costs are bounded, we normalize the cost matrix such that all values are between 0-1. We then determine the optimal coupling cost using the Sinkhorn algorithm. Note, we use the terms feature and label cost to refer to **dissimilarity in feature and label distributions**, respectively.

Algorithm 1 Computing Similarity of Datasets \mathcal{D}_1 and \mathcal{D}_2

Input: Datasets \mathcal{D}_1 and \mathcal{D}_2 , regularization parameter ϵ , normalization parameter λ

Output: Dataset similarity score between 0-1

procedure FEATURE COST CALCULATION

for each pair $(x_i, x_j) \in \mathcal{D}_1 \times \mathcal{D}_2$ **do**

if dimension ≥ 1000 **then**

 Embed data as in Section B.1

end if

 Calculate cosine similarity, $\rho(\cdot, \cdot)$, using MPC as in Section B.2

end for

procedure LABEL COST CALCULATION

for each label class pair $(y^c, y^{c'}) \in \mathcal{D}_1 \times \mathcal{D}_2$ **do**

 Estimate mean, μ , and covariance, Σ as in Section B.4

 Add zCDP noise as in Section B.3

 Compute Hellinger distance, $H^2(y^c, y^{c'})$ as in Equation A.1

end for

procedure CREATION OF TOTAL COST MATRIX

for each pair of feature-label points **do**

 Compute total feature-label cost

$$c(z_i, z_j) = \rho(x_i, x_j) + H^2(y_i^c, y_j^{c'})$$

end for

procedure OPTIMAL TRANSPORT CALCULATION

 Create a transportation map, π , as in Equation 3

 Calculate the overall similarity score

$$OT(\mathcal{D}_1, \mathcal{D}_2) = \frac{1}{\lambda} \sum_{z_i \in \mathcal{D}_1, z_j \in \mathcal{D}_2} c(z_i, z_j) \pi(z_i, z_j)$$

There are considerations and assumptions pertaining to several procedures:

- In FEATURE COST CALCULATION, when data have dimension ≥ 1000 , we recommend using compressed representations of the data. In most cases, this has the advantage of rendering the vectors linearly separable, thereby improving the ability of cosine similarity to accurately capture similarity between vectors.
- In LABEL COST CALCULATION, we assume label distribution follows a Gaussian distribution, as presented by Alvarez-Melis and Fusi (2020). This assumption is supported by the fact that the Gaussian approximation serves as an upper bound for the true cost and is effective for a wide range of labels (Gelbrich, 1990; Seddik et al., 2020).
- In OPTIMAL TRANSPORT CALCULATION, we have two hyperparameters, the regularization parameter for the Sinkhorn algorithm, ϵ ; and the normalization constant, λ . We recommend using a sufficiently low $\epsilon < 1e^{-2}$ to ensure the accuracy of the optimal transport mapping (Section D.6.1). For λ , we set it to 3 as the cosine similarity and Hellinger

Distance range from 0-2 and 0-1, respectively. In Section D.6.2 we show that our dataset similarity score is robust to a wide range of feature-to-label cost ratios.

5 Privacy-preserving Calculation

Data privacy is a necessary condition in cross-silo FL (Dayan et al., 2021). However, many existing dataset similarity methods cannot be calculated in a privacy-preserving manner. Our contribution lies in the development of a cost metric that can be calculated in a **provably secure and privacy-preserving manner with high accuracy and minimal computational overhead**. To achieve this, we implement a Multi Party Computation (MPC) protocol for feature cost that enables dot product calculation between two vectors securely (Du et al., 2004), and a zero-Concentrated Differential Privacy (zCDP) protocol for label cost that enables sharing of label distribution summary statistics in a privacy-preserving manner (Biswas et al., 2020) (see Sections A.1 and A.2 for details on MPC and zCDP, respectively). While we use existing privacy and security protocols, a thorough analysis of their combined implementation is essential to guarantee overall security and privacy preservation. In Section E.0.3, we provide a comprehensive analysis demonstrating that the released information through our combined protocol is guaranteed to be secure and private by not allowing for the reconstruction of the original datasets up to an orthonormal basis.

Our modifications to the OT cost function facilitate accurate and computationally efficient privacy-preserving and secure calculation. This greatly improves usability in federated settings. First, cosine similarity for feature cost requires only a dot product operation, which has a lightweight MPC protocol (Du et al., 2004). Importantly, this allows for pairwise sample-level comparison between datasets without sharing the data across site (See Section D.5 for computational complexity; for security guarantees, (see Du et al., 2004)). Second, using Hellinger Distance for label cost allows us to release only summary level statistics via zCDP. The approach introduced by Biswas et al. (2020), ensures accurate label cost calculation with low computational and sample complexity (for privacy guarantees (see Biswas et al., 2020)). In Figure D.2 we show that the use of these methods retains the accuracy and in Section D.5 we discuss computational complexity.

6 Theoretical Insights

Beyond its desirable privacy-preserving properties, our cost function is well-suited to predicting performance in FL without the need for computationally costly training. First, we discuss the suitability of cosine similarity and Hellinger distance for assessing feature and label costs, respectively. Then we justify their use within an OT framework. For the full proofs see Appendix C.

6.1 Cosine Similarity for Feature Cost

In high-dimensional spaces, cosine similarity, denoted as $1 - \cos(\theta_{x_i, x_j})$, is a particularly informative metric due to the *concentration of measure* phenomenon which offers a tight bound on the orthogonality of random vectors (Ledoux, 2001). In the context of data vectors in the same feature space, this means that non-orthogonality suggests that there exist shared signal between them.

Proposition 1: *For any pair of normalized vectors x_i and x_j drawn from two independent, high-dimensional datasets \mathcal{D}_i and \mathcal{D}_j , the probability that the cosine of the angle between them exceeds a threshold t is bounded by*

$$Pr(x_i \cdot x_j = |\cos(\theta_{x_i, x_j})| > t) < \frac{1}{nt^2}.$$

where n is the feature space dimension. This bound is valid when datasets are drawn from distinct and independent distributions. For full proof see Section C.1

Corollary: If the distributions have any overlap, this violates the independence assumption of the bound and vectors will exhibit non-orthogonality. This implies that non-orthogonal vectors in the same feature space share information. Other distance based measures do not have such tight bounds for independent datasets.

Now that we have established non-orthogonality between datasets as an indicator of shared information, we wish to connect the orientation of data vectors to weight divergence in FL. Consider data vector x_i and weights w with activation $\phi(x_i \cdot w)$. Their dot product determines the activation strength and model output, which contributes to the loss. Consequently, at client k , a gradient-based weight update depends on the orientation of the data vectors in that dataset relative to the weight vectors. As these vectors are typically normalized, this closely resembles cosine angle between them (Liu et al., 2017; Luo et al., 2018).

Proposition 2: *For normalized datasets, weight divergence in FL is bounded by the orientation of feature vectors across clients $c \in C$. Specifically, for any client k , the divergence in their weight updates with respect to the global model update, is given by*

$$|\Delta w^{Global} - \Delta w^k| \leq \left| \sum_{c=1}^C \alpha^c \sum_{x^c \in \mathcal{D}^c} \sum_{x^k \in \mathcal{D}^k} (\nabla_{\phi} L(x^c) - \nabla_{\phi} L(x^k)) (\sqrt{2(1 - \cos(\theta_{x^c, x^k}))}) \right|.$$

Δw is the model update, \mathcal{D}^c is the dataset for client c , $\nabla_{\phi} L(x^c)$ is the model gradient for client c , α^c is the contribution of client c such that $\sum_{c=1}^C \alpha^c = 1$. By having aligned samples between all clients $\in C$ and client k , we minimize $\sqrt{2(1 - \cos(\theta_{x^c, x^k}))}$. Note the term $\nabla_{\phi} L(x^c) - \nabla_{\phi} L(x^k)$ is also minimized when vectors that are aligned share the same label. This is accounted for in the label cost calculation. Similar to the bound of the weight divergence in Zhao et al. (2018), our bound also decomposes the divergence into a gradient difference term and a distribution difference term. The difference is that we quantify the distribution difference explicitly through the feature vector orientations. See Section C.2 for the full proof and discussion of the impact of non-linearities introduced in deep networks. See Section 7.5 for empirical validation.

6.2 Hellinger Distance for Label Cost

In FL, accurately comparing label distributions across datasets is crucial for understanding dataset similarity as label drift and class imbalances are common. As we model labels as distributions over features, we are mostly interested in comparing probability distributions rather than vectors in a space.

Remark 1: *Hellinger distance is a more appropriate measure for comparing label distributions than Euclidean distance.*

As Hellinger Distance is intrinsically connected to the Riemannian metric defined on the statistical manifold of probability distributions, it effectively captures the shortest geodesic distance in this manifold (Baktashmotlagh et al., 2014). Using Hellinger Distance shifts the focus from comparing probability densities in Euclidean geometry to within their statistical manifold, providing a more natural assessment for our purposes. Further, Hellinger Distance has the advantage of robustness and insensitivity to skew, which is important when comparing label classes in real-world data (Cieslak et al., 2012; Lindsay, 1994).

6.3 Feature and Label Costs Within the OT Framework

Proposition 3: *A hybrid cosine similarity-Hellinger distance cost function is admissible in the Optimal Transport framework.*

The original Wasserstein distance is a special case of (f, Γ) -divergence family, where Γ is all bounded 1-Lipschitz functions (Birrell et al., 2022). It is possible to replace Γ with another 1-Lipschitz function to change the interpretation from Euclidean geometry while retaining the optimal coupling properties. Both the feature and labels costs are 1-Lipschitz continuous and are therefore admissible Γ cost functions. For feature cost, as all sample vectors have been normalized, our cost function is then simply the dot product, which is 1-Lipschitz continuous. For label cost, the Hellinger Distance can be seen as applying the L2 norm to the square roots of probability measures. In our case, as we use well-defined probability distributions with bounded support to model label distributions (*e.g.*, Gaussian), the Hellinger Distance is also 1-Lipschitz continuous. By integrating these specific cost functions, we preserve the framework’s core principles, such as optimal mass redistribution, but with different geometrical and probabilistic implications that are better aligned with our goal of assessing dataset similarity.

7 Experiments

We now present experimental details and results for evaluating dataset similarity using our metric. We also compare our metric to the **original Wasserstein distance** with a Euclidean cost function. To test our dataset-agnostic claim, we include a variety of data types and tasks typically used in FL (Table 7, Section D.1 for full details). For each dataset, we assess the performance of five different training algorithms: (1) Single site training (each site trains a separate model) which serves as our baseline. (2) Joint training where one model is trained on the combined datasets. (3) FL using FedAvg (McMahan et al., 2017). (4) FL using Personalized Federated Learning with Moreau Envelopes, *i.e.*, pFedME (T Dinh et al., 2020). (5) FL using Ditto (Li et al., 2021). pFedME and Ditto are two popular personalized FL algorithms. The code for data partitioning, calculation of dataset similarity, and model training can be found at github.com/anonymous-submissions/ot_cost.

7.1 Synthetic Dataset

To gain a clear understanding of our metric’s behavior, we first evaluate it on a synthetic dataset. The synthetic dataset allows us to precisely control distribution shifts and systematically evaluate a range of scenarios. Our approach involves drawing samples from two distinct distributions, varying how much overlap in distributions the datasets share. We can achieve similarity scores between 0-1 using this technique and find the following:

Dataset	Description	Metric
Synthetic	Dataset with controlled distribution shifts	F1-score
Credit	Fraud prediction	F1-score
Weather	Temperature prediction	R^2
ExtendedMNIST	Handwritten digit & character classification	Accuracy
CIFAR	Object classification	Accuracy
IXITiny*	Image segmentation of 3D-brain MRIs	DICE
ISIC2019*	Dermoscopy skin lesion classification	Balanced Accuracy

Table 1: Summary of datasets used

*Real-world medical imaging datasets collected from multiple sites

1. When datasets are drawn from the same distribution, we obtain a score of 0.03 and find an improvement in model performance from FL (Figure 1).
2. When datasets are drawn from distinct distributions, we obtain a score of 0.5 and find worsened performance from FL. As discussed in Section 6.1, this is not surprising as we expect data vectors to be orthogonal when they are unrelated (Figure 1).
3. When datasets are drawn from antipodal distributions¹, we obtain a score of 0.9 and find extreme negative learning from FL (Figure D.2).

7.2 Benchmark Datasets

Next, we evaluate the metric on benchmark datasets: Weather, Credit, ExtendedMNIST, and CIFAR-10. This allows us to replicate the models and distribution shifts presented in many FL papers. Our findings confirm observations from the synthetic dataset; **scores ≤ 0.2 generally result in improved FL performance, while scores ≥ 0.3 lead to a decline in model performance** compared to the baseline (Figure 1). This finding is consistent across all datasets and models, highlighting the robustness of our similarity metric.

7.3 Real-world Datasets

To validate our metric’s ability to capture real-world differences across datasets and the impact of these differences on FL performance, we tested it on two medical imaging datasets: IXITiny, an image segmentation task on 3D brain MRIs, and ISIC2019, a skin lesion classification task using dermoscopy images. Both datasets have **natural non-IID partitions** as they are both made up of samples collected from different sites using different machines. We compared performance across different pairs of sites with differing dataset similarity scores. We obtain results consistent with the benchmark and synthetic datasets.

As both datasets have real-world partitions, is also useful to determine if our metric accurately captures what is known.

- For IXITiny, we find that the scores produced by our metric aligned with the data collection practices. Two sites used similar Philips MRI machines with comparable imaging parameters, while the third site employed a different GE machine with unspecified

1. Mutually exclusive distributions that ensure the data vectors point in opposing directions.

settings (Brain-development.org). The metric assigned a low score of 0.08 between the two Philips sites, indicating high similarity, and higher scores of 0.28 and 0.30 between the GE site and the other two, respectively. This finding is consistent with the observations from Ogier du Terrail et al. (2022).

- For ISIC2019, we find that our score aligns with how the data was collected while also providing some novel insights. ISIC2019 data is collected from four sites (two in Europe, one in USA, one in Australia). One of the European sites uses three different machines, resulting in separate data partitions. We find that European sites have lower scores with each other than with Australian and American sites, consistent with the findings in Ogier du Terrail et al. (2022). Interestingly, the metric revealed that the choice of imaging machine within the same European site had a more substantial impact on dataset similarity than the geographical location. Datasets from different European sites using the same machines were more similar than datasets from the same site using different machines. A similar finding was found by Wen et al. (2022).

Although the differences in these datasets are well-documented, our metric offers significant utility when they are not known. This information can guide the selection of sub-networks of sites with similar datasets for collaboration, potentially leading to improved FL performance. Additionally, in cases like medical imaging, the metric can inform the extent of data pre-processing steps needed to normalize samples and mitigate the negative effects of non-IID data. For instance, the metric could highlight the need for image normalization and standardization to address differences in imaging equipment or protocols across institutions.

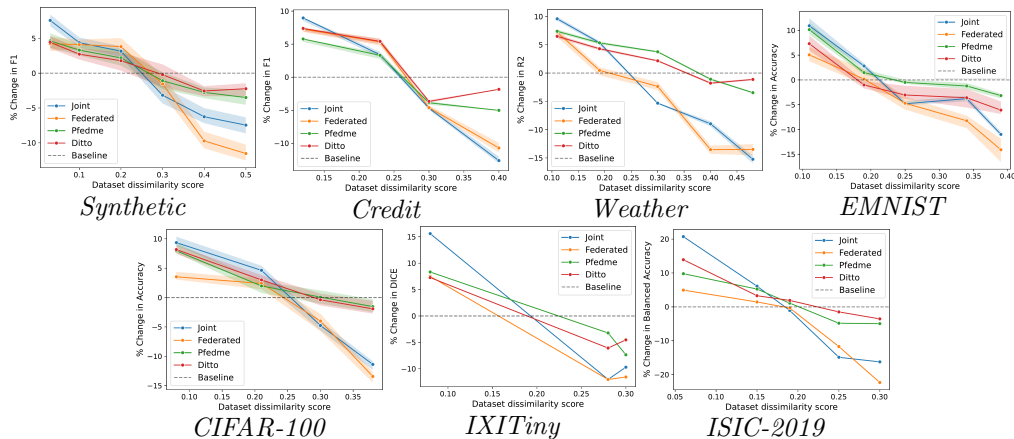


Figure 1: **Performance of models trained on datasets with different scores.** Results expressed as percentage changes from single baseline with Joint (blue), FedAvg (orange), pFedME (green) and Ditto (Red)

7.4 Impact of Personalized FL Algorithms

When comparing the performance of personalized FL algorithms (pFedMe and Ditto) to FedAvg, we find that they offset the negative effects of high dissimilarity between datasets,

while retaining performance when datasets are similar. However, these results are highly sensitive to the regularization parameter used which requires a hyperparameter grid search. **We find that our metric exhibits a correlation with the regularization parameters** used in pFedMe and Ditto (Section D.1.1). When datasets are more similar (lower score), performance is improved with larger regularization that promotes federation. Conversely, when datasets are dissimilar (higher score), performance is improved with less regularization, promoting personalization. This suggests that the metric can be used to guide choices on whether personalized FL algorithms would be useful and support hyperparameter selection.

7.5 Relationship to Weight Divergence

To gain further insight into relationship between our metric and FL performance, we measure weight divergence (Equation 1) for models trained using FedAvg (Figure 2). Our findings demonstrate a correlation between weight divergence and our metric. Datasets with higher dataset dissimilarity result in greater divergence, and this divergence manifests for longer. Importantly, our metric predicts this behavior without model training. While such a relationship can be expected for any Lipschitz-bounded function, we find that our metric has a higher correlation with weight divergence than the original Wasserstein distance across all datasets (paired t-test, $p = 0.013$, Section D.4). This suggest that our metric more tightly captures training dynamics without the need for model training.

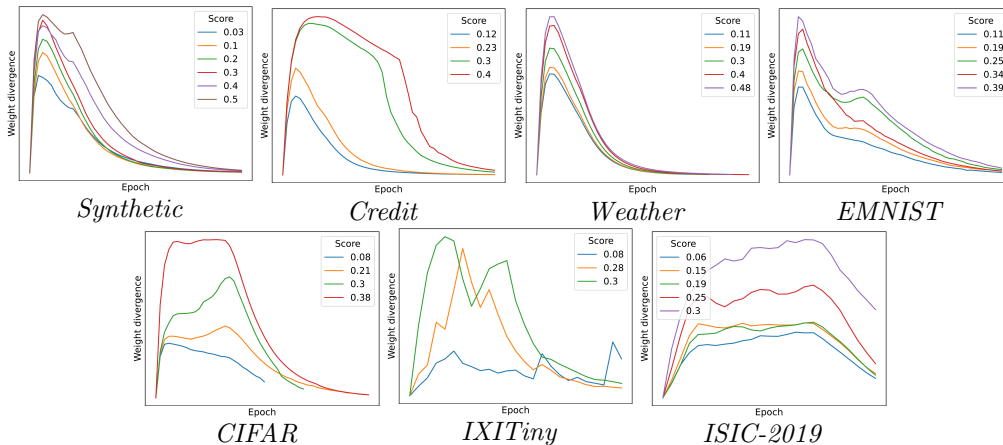


Figure 2: **Weight divergence during training for FedAvg models**

7.6 Sample Size Complexity

Our algorithm for dataset similarity metric is also sample size efficient. This is important in FL, where dataset size in individual sites is limited (see Mena and Niles-Weed, 2019; Genevay et al., 2019, for theoretical bounds). Figure 3 presents a comparison of the estimated dataset similarity scores on the full datasets vs. subsampled datasets. We show that even for high dimensional datasets, accurate estimates can be achieved with $\sim 1,000$ samples.

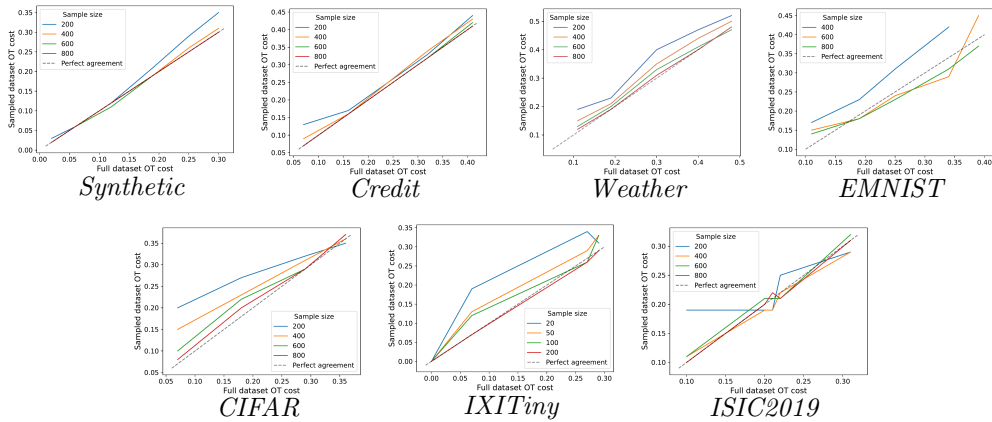


Figure 3: Scores calculated from full dataset and subsampled dataset. Dashed $Y=X$ represents perfect agreement.

7.7 Comparison to Original Wasserstein Distance

Our metric offers three key advantages for FL compared to the original Wasserstein distance: enhanced interpretability, greater relevance to training dynamics, and computationally efficient privacy preservation. Firstly, unlike original Wasserstein distance, our metric provides a consistent interpretation of similarity across datasets of varying dimension and scale. To illustrate the issue of inconsistent interpretation, consider Figure 4 which shows results using the original Wasserstein distance. While both metrics show a connection between increasing scores and performance, the key difference is interpretability. A cost of $\sim 1e^8$, can imply improved learning in one dataset (IXITiny) but negative learning in another (ISIC2019). Conversely, our metric consistently shows that in both tasks, scores ≤ 0.2 indicate improved FL performance whereas scores ≥ 0.3 indicates worsen FL performance. Second, our metric is more tightly coupled with weight divergence, a key factor influencing FL performance. As demonstrated in Section 6.1, the cosine similarity component of our metric directly measures the alignment of data point orientations across datasets, which, in turn, captures weight divergence during training. Finally, our metric can be computed in a privacy-preserving manner with low computational overhead (Section D.5). To date, no such privacy-preserving solution for the original Wasserstein distance exists.

Limitations: There are several limitations to our current approach. First, our metric assumes concordant features across the datasets. Future work could explore how our metric performs when datasets have different features. It is worth noting, however, that in FL, datasets typically share the same feature space. Second, the computational complexity of our metric increases with the dataset dimensionality. Third, the use of cosine similarity limits our ability to capture non-linear relationships within the features. The latter two limitations can be addressed by embedding the datasets to reduce dimensionality and ensuring linear separability of vectors prior to similarity computation. Our successful results with CIFAR, IXITiny, and ISIC2019 datasets support the viability of this approach. Finally, we modeled

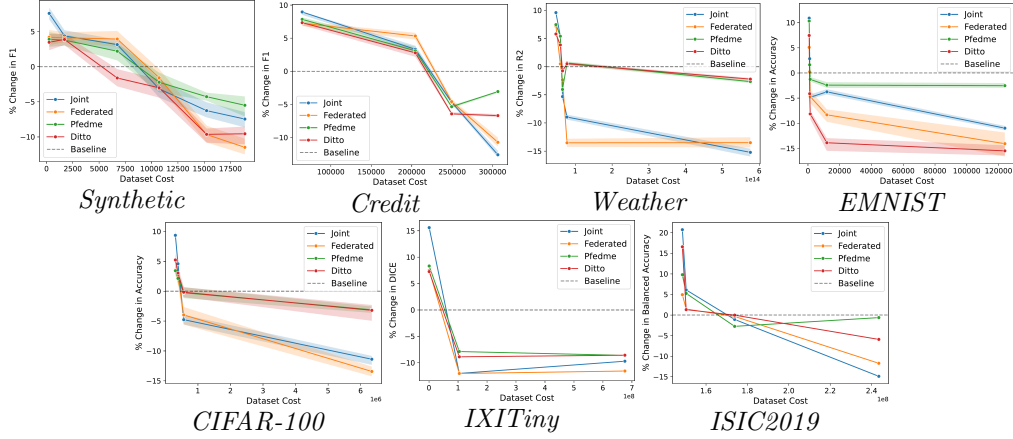


Figure 4: **Performance of models trained on datasets with different original Wasserstein distances.** Results expressed as percentage change from a single model baseline with Joint (blue), FedAvg (orange), pFedME (green), and Ditto (Red).

the label distributions as Gaussian. While this assumption held well for our datasets, it may not be suitable for all scenarios.

Acknowledgments and Disclosure of Funding

This work was funded by grants R00HG01090 and R35GM147004 to GG

Appendix A. Background

This section includes preliminary information for Hellinger distance and privacy-preserving techniques.

A.1 Hellinger Distance

The Hellinger Distance (HD) is a measure of similarity between two probability distributions (Chen et al., 2023; González-Castro et al., 2013). Given two probability distributions, P and Q , defined over the same domain \mathcal{X} , HD can be calculated as

$$H^2(P, Q) = \frac{1}{2} \int_{\mathcal{X}} \left(\sqrt{P(dx)} - \sqrt{Q(dx)} \right)^2.$$

For two Gaussian distributions, HD has the closed form solution

$$1 - \frac{|\Sigma^c|^{\frac{1}{4}} |\Sigma^{c'}|^{\frac{1}{4}}}{|\frac{1}{2}\Sigma^c + \frac{1}{2}\Sigma^{c'}|^{\frac{1}{4}}} \exp\left[-\frac{1}{8} \mu^\top \left(\frac{1}{2}\Sigma^c + \frac{1}{2}\Sigma^{c'}\right)^{-1} \mu\right]$$

where μ and Σ are the mean and covariance matrix.

A.2 Secure Multiparty Computation

Secure multiparty computation (MPC) is a cryptographic technique that enables multiple parties to jointly compute a function without revealing their inputs to each other (Evans et al., 2018). The advantage of MPC is its ability to protect inputs against both outside adversaries and other involved parties, while producing accurate outputs.

A.3 Differential Privacy

Differential privacy is a formal standard for protecting individual privacy in statistical data analysis. It has two forms pure and approximate. Pure DP is parameterized by one parameter, ϵ , that quantifies the allowable privacy loss a sample may experience (Dwork et al., 2014). The formulation for pure DP is

$$\frac{\Pr[F(x) = S]}{\Pr[F(x') = S]} \leq e^\epsilon$$

where x and x' are neighbouring datasets differing by at most one sample, $F(\cdot)$ is a function applied to the dataset, and S is the output. e^ϵ is the multiplicative factor where a lower ϵ represents greater privacy guarantees. Approximate or (ϵ, δ) -DP is a more flexible variant that guarantees that the probability of exceeding the privacy loss bound specified by ϵ is at most δ (Dwork and Rothblum, 2016). The formulation for approximate-DP is

$$\Pr[F(x) = S] \leq e^\epsilon \Pr[F(x') = S] + \delta.$$

When $\delta = 0$, pure and approximate-DP are equivalent.

zero-concentrated DP (zCDP) is a relaxation of pure DP that provides tighter analytic bounds on the privacy loss given certain assumptions are made on the distribution (Bun and Steinke, 2016). A randomized mechanism satisfies zCDP if for all neighboring datasets and all $\alpha \in (1, \infty)$

$$D_\alpha(F(x)||F(x')) = \frac{1}{\alpha - 1} \log E \left(\frac{\Pr[F(x) = S]}{\Pr[F(x') = S]} \right)^\alpha \leq \rho\alpha.$$

Here, the first term is the R enyi divergence, a generalized measure of divergence between probability distributions, x and x' are neighbouring datasets differing by at most one sample, $F(\cdot)$ is a function applied to the dataset, S is the output, ρ is the privacy parameter, and α is a tuning parameter that adjusts the sensitivity of the privacy guarantee. zCDP permits sharper analysis when the mechanism is Gaussian with small mean (Bun and Steinke, 2016; Dwork and Rothblum, 2016). To convert between ρ and ϵ, δ one can use the following formula (Near and Abuah, 2021)

$$\epsilon = \rho + 2\sqrt{\rho \log\left(\frac{1}{\delta}\right)}.$$

Appendix B. Algorithm

This section describes our algorithm in more detail.

B.1 Embedding process

When working with high-dimensional data (≥ 1000), embeddings can provide a more compact and efficient representation. In our experiments, this threshold has proven effective, although it remains a heuristic recommendation. We apply this approach for three datasets.

- **CIFAR**: We train an autoencoder and test bottleneck sizes of 250, 500, 750, 1,000, and 2,000, selecting 1,000.
- **IXITiny**: We train an autoencoder with 4 layers and tested bottleneck sizes of 256, 512, 1,024, 2,048 and 4,960, selecting 2,048. Rather than recreating the image, we recreate the bottleneck representation from a pretrained 3D Unet (Pérez-García et al., 2021).
- **ISIC2019**: We use a pre-trained autoencoder which has bottleneck dimension of 18,432 (Zenn, 2021).

B.2 MPC protocol

Our MPC protocol to calculate the dot product in a privacy preserving way is adapted from Du et al. (2004).

Site 1 hold dataset $A \in \mathbb{R}^{N_1 \times d}$, Site 2 hold dataset $B \in \mathbb{R}^{N_2 \times d}$ where d is # features, N_i is # samples.

1. Server creates $M_{d \times d}$ using Reed-Hoffman encoding and sends M to Site 1 and M^{-1} to Site 2.
2. Site 1 computes $A_1 = A \times M_{\text{left}}$, $A_2 = A \times M_{\text{right}}$ and sends A_1 to the server.
3. Site 2 computes $B_1 = B \times M_{\text{top}}^{-1}$, $B_2 = B \times M_{\text{bottom}}^{-1}$ and sends B_2 to the server.
4. Server sends B_2 to Site 1 and A_1 to Site 2.
5. Site 1 computes $V_a = A_2 \times B_2$ and sends it to the server.
6. Site 2 computes $V_b = A_1 \times B_1$ and sends it to the server.

We have $\mathbf{AB} = AMM^{-1}B = \begin{pmatrix} A_1 & A_2 \end{pmatrix} \begin{pmatrix} B_1 \\ B_2 \end{pmatrix} = V_a + V_b$.

The method requires construction of a secure random invertible matrix, M . This can be generated using maximum distance separable (MDS) codes such as Reed-Solomon codes. MDS codes ensure that any subset of columns are linearly independent of each other such that it is impossible to recover the original data (MacWilliams, 1977).

B.3 zCDP protocol

We use COINPRESS developed by Biswas et al. (2020), which enables release of the mean and covariance matrices of multivariate data. For a technical explanation of the method

including privacy guarantees (see Biswas et al., 2020). The method requires the user to input *a priori* knowledge of the data including starting values and a search radius. We use the actual label class mean and covariance for starting values and a search radius of 1. This is possible as our ‘population’ is the dataset. This allows us to use $\rho = 0.1$ ($\epsilon = 0.99, \delta = 0.01$) which provides strong privacy guarantees (NIST, 2022).

B.4 Label cost calculation

The label distance calculation requires the inversion of covariance matrices. For high-dimensional and sparse datasets with singular covariance matrices, this results in degenerate matrices. To avoid this, we use PCA to reduce the dimensionality of the covariance matrices, retaining 80% of the explained variance. Importantly, for privacy preservation, we fit the principal components on one covariance matrix and apply the same transformation to the other, eliminating the need to share raw data. If both covariance matrices need fitting together, we suggest using Federated PCA (Grammenos et al., 2020).

Appendix C. Theoretical Insights

In this section we provide full proofs for our theory linking cosine similarity of data vectors and weight divergence in FL.

C.1 Bound of orthogonality

Outline: In this proof we aim to bound the cosine angle between two random vectors sampled from independent datasets. The goal is to show that non-orthogonality in two datasets with the same feature space is indicative of shared information. We extend the theorem from random vectors on a hypersphere to random vectors from two datasets.

PRELIMINARIES

The proof relies on the following preliminaries:

1. A random unit vector $x = (x_1, x_2, \dots, x_n)$ on the the unit hypersphere of \mathbb{R}^n can be approximated by randomly choosing each coordinate, x_k from the set $\{1, -1\}$ for $\forall k \in 1, \dots, n$ and then scaling by $\frac{1}{\sqrt{n}}$. Taking all coordinates $x_k \in \{1, -1\}$ is equivalent to assuming each coordinate, k , has a shifted and scaled Bernoulli distribution with $p = 0.5$. Note that we relax this assumption later in the proof. ²
2. A random unit vector inside the unit ball of \mathbb{R}^n will almost surely be on the surface as the dimension of the unit ball, n , increases:

- We define a unit ball $B_n := \{(x_1 \dots x_n) : \sum x_i^2 \leq 1\}$ has volume $v(B_n) = \frac{\pi^{\frac{n}{2}}}{\Gamma(\frac{n}{2} + 1)}$. As $n \rightarrow \infty, v(B_n) \rightarrow 0$.

2. An exact way to select a random point on the surface is to choose x_k from $\sim N(0, 1)$ and normalizing by $\frac{1}{(\sum_k x_k^2)^{0.5}}$. In high dimensions, the simpler Bernoulli method approximates this well.

- The majority of the volume in B_n is concentrated in a thin strip S_n of width $O(\sqrt{\frac{\log n}{n}})$ around its boundary. Specifically, the volume in B_n outside of this strip is approximately $1 - \frac{1}{c}$ for any $c > 1$ where c is a scaling factor. This is the "concentration of measure" phenomenon in high dimensions.
3. Consider two random vectors on the unit hypersphere in \mathbb{R}^n , denoted as x_i and x_j . The dot product of these vectors is $x_i \cdot x_j = |x_i||x_j|\cos(\theta)$ where θ is the angle between them. As x_i and x_j are both on the unit hypersphere, $|x_i| = |x_j| = 1$, so $x_i \cdot x_j = \cos(\theta)$.

LEMMA 1: A FIXED VECTOR AND ANY RANDOM VECTOR ON THE SURFACE ARE ALMOST-ORTHOGONAL

Suppose a is a fixed unit vector in \mathbb{R}^n . Let x be a random vector with $x_k \in \{1, -1\}$ such that $x = \frac{1}{\sqrt{n}}(x_1, \dots, x_n)$. Then, let $X = a \cdot x = \sum_{k=1}^n a_k x_k$ such that $Pr(|X| > t) = Pr(\cos\theta_{a,x} > t)$. Then $E[X] = E[\sum a_i x_i] = 0$ and $Var[X] = E[(\sum a_i x_i)^2] - 0 = \sum a_i^2 E[x_i^2] = \sum \frac{a_i^2}{n} = \frac{1}{n}$. Assuming X is normally distributed, the Chebyshev inequality of X is

$$Pr(|X| > t) < \frac{\frac{1}{n}}{t^2} = \frac{1}{nt^2}.$$

As $n \rightarrow \infty$, $Pr(|X| > t) \rightarrow 0$. To use the Chebyshev inequality, we invoke the central-limit theorem, applicable when $n \rightarrow \infty$.

LEMMA 2: ANY 2 RANDOM VECTORS ON THE UNIT HYPERSPHERE ARE ALMOST ALWAYS ORTHOGONAL BASED ON CONCENTRATION OF MEASURE

Assume x_i and x_j are unit vectors drawn from a uniform distribution in the unit hypersphere. If we take $X_{i,j} = x_i \cdot x_j$ to be a point that lies in the ball. Given the concentration of measure phenomenon mentioned in the preliminaries, the absolute value of $X_{i,j}$ is most likely approximately 0. Specifically, with probability greater than $1 - \frac{1}{n}$, the absolute value of $X_{i,j}$ is bounded by $O(\sqrt{\frac{\log n}{n}})$. The fraction of the volume of the unit ball lying outside the strip around the surface, where the absolute value of $\cos\theta_{x_i, x_j}$ exceeds $\sqrt{\frac{\log n}{n}}$, is less than $\frac{1}{n}$. Thus, we have

$$Pr\left(|\cos(\theta_{x_i, x_j})| > \sqrt{\frac{\log n}{n}}\right) < \frac{1}{n}.$$

As $n \rightarrow \infty$ there is high probability every pair of vectors has inner product ≈ 0 .

PROOF 1: ANY PAIR OF VECTORS SAMPLED FROM 2 RANDOM DATASETS ARE ALMOST ALWAYS ORTHOGONAL

While Lemma 2 gives us intuition into the concentration of measure phenomenon, it is limited to random vectors uniformly sampled from the unit hypersphere. To extend the proof to vectors sampled from 2 random datasets, we can no longer assume the vectors are uniformly drawn from the unit hypersphere. Instead we assume that $\mathcal{D}_1 \in \mathbb{R}^{n_1 \times f}$ and $\mathcal{D}_2 \in \mathbb{R}^{n_2 \times f}$ where n is the number of samples and f is the number of features. We assume that the datasets are drawn from two distinct and independent distributions, *i.e.*,

the 2 datasets share no information, and that both datasets have been standardized (a common practice in deep learning tasks). If we take x_i and x_j as vectors that come from datasets \mathcal{D}_1 and \mathcal{D}_2 such that $x_i \sim N(0, \Sigma_1)$ and $x_j \sim N(0, \Sigma_2)$. As \mathcal{D}_1 and \mathcal{D}_2 are drawn from distinct and independent distributions, their covariance matrices are also independent. Note that Σ_1 and Σ_2 are not necessarily diagonal matrices, implying that the components of the vectors in each dataset are not always independent. Using Lemma 1 and the fact the two vectors are independent of each other, $E[x_i \cdot x_j] = E[x_i]E[x_j] = 0$ and $Var[x_i \cdot x_j] = E[(x_i \cdot x_j)^2] - 0 = E\left[\left(\sum_{k=1}^f x_{ik}x_{jk}\right)^2\right] = \sum_{k=1}^f E[x_{ik}^2]E[x_{jk}^2]$. This final simplification holds as the two vectors are independent with no covariance. As the features are symmetrically distributed about 0 with a variance of 1 due to Z-score normalization $E[x_{ik}^2]E[x_{jk}^2] \approx 1$. Then, using the Chebyshev inequality and the central limit theorem (applicable as $f, n \gg 30$), we can bound the probability that the absolute value of the cosine of the angle between a pair of randomly drawn vectors from the two datasets exceeds a threshold t

$$Pr(|\cos(\theta_{x_i, x_j})| > t) < \frac{Var[x_i \cdot x_j]_{\frac{1}{n}}}{t^2} \approx \frac{1}{nt^2}.$$

Note this holds as the datasets are independent with *no shared information*. However, if the datasets are not independent due to underlying common features, this bound no longer holds and we expect randomly drawn vectors to be non-orthogonal. Note similarly to Lemma 2, this orthogonality holds as $n \rightarrow \infty$. In particular, it must scale as a function of dataset size.

C.2 Weight Divergence in FL

Outline: Now we link model updates to the relative orientation of data vectors. We then show that when vectors from independent datasets are oriented differently, weight divergence occurs. This motivates our choice of cosine similarity to measure feature cost.

PRELIMINARIES

1. Update steps in gradient descent are given by the equation $w^{i+1} := w^i - \eta \nabla_w L$ where $\nabla_w L$ denotes the gradients with respect to the weights, and η is the learning rate.
2. Using the chain rule, for a 1 layer network, we can decompose $\nabla_w L$ further to $\nabla_w L = \frac{\partial L}{\partial \phi} \cdot \phi'(w \cdot x) \cdot x$ where ϕ' is the derivative of the activation function. This can be used to decompose multi-layer networks as well.
3. Each input data point x can be broken into two components, one that is parallel to the weight vector w , denoted x_{\parallel} , and one that is perpendicular, denoted x_{\perp} . Formally, we express this as $x = x_{\parallel} + x_{\perp}$, where $x_{\parallel} = \frac{(x \cdot w)w}{\|w\|^2}$ and $x_{\perp} = x - x_{\parallel}$.
4. When vectors a, b, c are normalized (*i.e.*, $\| \cdot \| = 1$), the cosine similarity, or dot product, follows the following inequality $|\cos(a, b) - \cos(a, c)| \leq \sqrt{2(1 - \cos(b, c))}$. This is arrived at by using the Cauchy Schwarz inequality $|a \cdot (b - c)| = |a \cdot b - a \cdot c| \leq \|a\| \|b - c\| = \|b - c\|$ and $\|b - c\|^2 = \|b\|^2 + \|c\|^2 - 2b \cdot c = 2(1 - \cos(b, c))$.

LEMMA 3: WEIGHT UPDATE IS PROPORTIONAL TO THE PARALLEL COMPONENT OF THE INPUT VECTOR

Let $g = \nabla_w L$. In a one-layer network, we can express g in terms of the input vector, $g = \nabla_{\phi} L \cdot \phi'(w \cdot x) \cdot x$. Decomposing x leads to $g = \nabla_{\phi} L \cdot (\phi'(w \cdot (x_{\parallel} + x_{\perp}))(x_{\parallel} + x_{\perp})) = \nabla_{\phi} L \cdot (\phi'(w \cdot x_{\parallel})x_{\parallel} + \phi'(w \cdot x_{\perp})x_{\perp})$. However, $w \cdot x_{\perp} = 0$ so we get $g = \nabla_{\phi} L \cdot \phi'(w \cdot x_{\parallel})x_{\parallel}$. Assuming we are in the linear region of the ReLU activation function and so $\phi'(w \cdot x_{\parallel}) = 1$, this leaves us with

$$\Delta w \propto g = \nabla_{\phi} L \cdot x_{\parallel}.$$

Hence, the update to w is proportional to the component of the input vector x that is parallel to w , scaled by the gradient of the loss with respect to the activation function output. Note in a multi-layered network we replace $g = \nabla_{\phi} L \cdot \phi'(w \cdot x_{\parallel})x_{\parallel}$ with $g \propto f(k') \nabla_{\phi} L \cdot \phi'(w \cdot x_{\parallel})x_{\parallel}$ where $f(k')$ is a function that encapsulates the chain of derivative products with respect to deeper layers. Importantly, even in the multi-layer case, there is still a dependence on x_{\parallel}

Remark 2:

- In deeper networks, this relationship may only hold in the early layers. However, it has been shown that early layers function to extract fundamental features from the dataset that are used by deeper layer (Zeiler and Fergus, 2014; Yosinski et al., 2015). Thus, the relationship will still have implications for a deeper network.
- Further, assuming neural networks act as a mapping function from input space X to output space Y and that this function is Lipschitz continuous, we can invoke the smoothness assumption. Formally, $\exists K : \forall x_1, x_2 \in X \Rightarrow d_Y(f(x_1), f(x_2)) \leq K d_X(x_1, x_2)$. This essentially means that data points which are proximate in the feature space will continue to remain close in the output space, even when subjected to the non-linear transformations of the model
- Early during training most networks are initialized such that $w \cdot x$ is in the linear region of the activation function which is where updates occur (He et al., 2015; Heaton, 2018). While this may breakdown over training, the direction of early training has consequences for the final model.

LEMMA 4: THE TOTAL CHANGE IN w IS PROPORTIONAL TO THE SUMMED PARALLEL COMPONENT OF ALL VECTORS IN DATASET \mathcal{D}

Let's consider data vectors $x \in \mathcal{D}$. The total loss for these data points is $L = \sum_{x \in \mathcal{D}} L(x)$. Using the fact that the derivative of a sum is the sum of the derivatives, we get $\nabla_w L = \sum_{x \in \mathcal{D}} \nabla_w L(x)$. From our previous analysis we get that

$$\Delta w \propto \sum_{x \in \mathcal{D}} \nabla_{\phi} L(x) \cdot x_{\parallel}. \tag{C.1}$$

Note, we assume that the constant of proportionality is the same for all vectors. This constant is impacted by η and $\phi'(\cdot)$. For a given training round, η remains the same for all vectors. Further, with random or He initialization of weights, the expected value of $\phi'(\cdot)$ should be similar for all vectors.

PROPOSITION 2: FOR NORMALIZED DATASETS, WEIGHT DIVERGENCE IN FL IS BOUNDED BY THE ORIENTATION OF FEATURE VECTORS ACROSS CLIENTS $c \in C$

We use the previous result (Equation C.1) but replace x_{\parallel} with $\|x\| \cos(\theta_{xw})$ where θ_{xw} is the angle between the weight and feature vector. As $\|x\| = 1$ this simplifies to $\cos(\theta_{xw})$. Then

$$\Delta w \propto \sum_{x \in \mathcal{D}} \nabla_{\phi} L(x) \cos(\theta_{xw}).$$

The global weight update across all clients $c \in C$ is

$$\Delta w^G = \sum_{c=1}^C \alpha^c \Delta w^c \propto \sum_{c=1}^C \alpha^c \sum_{x \in \mathcal{D}^c} \nabla_{\phi} L(x^c) \cos(\theta_{x^c w}).$$

where α^c is the contribution of client c to the global model and $\sum_{c=1}^C \alpha^c = 1$. Now we quantify the weight divergence between client k and global model G

$$|\Delta w^G - \Delta w^k| \propto \left| \sum_{c=1}^C \alpha^c \sum_{x^c \in \mathcal{D}^c} \nabla_{\phi} L(x^c) \cos(\theta_{x^c w}) - \sum_{x^k \in \mathcal{D}^k} \nabla_{\phi} L(x^k) \cos(\theta_{x^k w}) \right|.$$

We now wish to create a direct comparison between data vectors from all clients but this is not directly possible. However, we can approximate the equation using a pairwise comparison across all data vectors in the datasets and then pair vectors based on high similarity. The full pairwise comparison then acts as an upper bound

$$|\Delta w^G - \Delta w^k| \leq \left| \sum_{c=1}^C \alpha^c \sum_{x^c \in \mathcal{D}^c} \sum_{x^k \in \mathcal{D}^k} \nabla_{\phi} L(x^c) \cos(\theta_{x^c w}) - \nabla_{\phi} L(x^k) \cos(\theta_{x^k w}) \right|.$$

Utilizing the distributive property of multiplication over subtraction we get

$$|\Delta w^G - \Delta w^k| \leq \left| \sum_{c=1}^C \alpha^c \sum_{x^c \in \mathcal{D}^c} \sum_{x^k \in \mathcal{D}^k} (\nabla_{\phi} L(x^c) - \nabla_{\phi} L(x^k)) (\cos(\theta_{x^c w}) - \cos(\theta_{x^k w})) \right|.$$

Note, this step assumes that the gradients are Lipschitz continuous and that differences in gradients and cosine similarity of feature vectors to the weights interact linearly. This is an acceptable assumption as all clients share the same weights and loss function. Then using the inequality in preliminary 6

$$|\Delta w^G - \Delta w^k| \leq \left| \sum_{c=1}^C \alpha^c \sum_{x^c \in \mathcal{D}^c} \sum_{x^k \in \mathcal{D}^k} (\nabla_{\phi} L(x^c) - \nabla_{\phi} L(x^k)) (\sqrt{2(1 - \cos(\theta_{x^c x^k}))}) \right|.$$

We now have a bound that's based on the relative orientation of feature vectors to weight divergence. It can be seen that weight divergence is minimized when the feature vectors are perfectly oriented together between datasets.

Corollary 2: This pairwise comparison is equivalent to constructing a pairwise matrix, M , across all data points in client k with all other clients $\in C$ such that each entry of M is

$$M_{ij} = |\nabla_{\phi} L(x)^c - \nabla_{\phi} L(x)^k \cdot \sqrt{2(1 - \cos(\theta_{x^c x^k}))}|.$$

M is an upper bound that is pairwise across all costs. However, it is more appropriate to have a sample-to-sample mapping between the datasets. This is because data vectors appear once in a training update. To achieve this mapping we can take the minimum coupling, π .

$$\arg \min_{\pi \in \Pi} \sum_{i,j} \pi_{i,j} M_{i,j}$$

where π satisfies the constraints of mass conservation between datasets \mathcal{D}^c and \mathcal{D}^k .

Limitations: The proofs rely on simplifying assumptions that do not capture the complexities of deeper networks which are impacted by other factors. Rather, our goal is to show that relative feature orientation plays an important role in weight divergence.

Appendix D. Experiments

In this section we describe in more detail the experimental setup and present additional results referenced in the main manuscript. All dataset processing, models and hyperparameters are available at github.com/annonymous-submissions/ot_cost.

D.1 Setup: Datasets, Training, and models

Table D.1 describes how we partitioned datasets to produce datasets with specific dataset dissimilarity scores. We employ a mixture of feature and label skew Hsieh et al. (2020); Zhao et al. (2018).

- **Synthetic:** We draw samples from 2 distinct distributions, \mathcal{D}_a and \mathcal{D}_b . For partition 1 we always draw samples from \mathcal{D}_a and for partition 2 we vary the proportion of samples drawn from \mathcal{D}_a and \mathcal{D}_b .
- **Credit:** We introduce increasing amounts of label skew and feature noise to the datasets. Label skew is achieved by introducing label distribution bias. For example, a 10% bias means 10% more positive labels and negative labels in partition 1 and 2, respectively. Feature noise is achieved by adding Gaussian noise.
- **Weather:** We partition datasets based on climate as described by Malinin et al. (2022). This introduces real-world feature and label skew.
- **EMNIST:** We partition datasets based on labels.
- **CIFAR:** We partition the dataset based on labels.
- **IXITiny:** We partition based on site. This is a natural partition. Sites Guys and Hammersmith use a Philips system with similar settings. Site IOP uses a GE system with unknown settings (see [Brain-development.org](https://brain-development.org); Ogier du Terrail et al., 2022).
- **ISIC2019:** We partition based on site. This is a natural partition.

D.1.1 Setup: Training and Models

For each combination of dataset, cost, and training, we performed learning rate and optimizer tuning via grid search. We evaluate five learning rates ($5e^{-1}, 1e^{-1}, 5e^{-2}, 1e^{-2}, 5e^{-3}, 5e^{-4}$) and two optimizers (ADAM and SGD). The SGD optimizer is exclusively used for federated

Dataset	OT score	Partition 1	Partition 2
Synthetic	0.00*	100% \mathcal{D}_a	Identical to Partition 1
	0.01*	100% \mathcal{D}_a	50% subset of Partition 1
	0.03	100% \mathcal{D}_a	100% \mathcal{D}_a
	0.1	100% \mathcal{D}_a	85% \mathcal{D}_a , 15% \mathcal{D}_b
	0.2	100% \mathcal{D}_a	65% \mathcal{D}_a , 35% \mathcal{D}_b
	0.3	100% \mathcal{D}_a	43% \mathcal{D}_a , 57% \mathcal{D}_b
	0.4	100% \mathcal{D}_a	25% \mathcal{D}_a , 75% \mathcal{D}_b
	0.5	100% \mathcal{D}_a	11% \mathcal{D}_a , 89% \mathcal{D}_b
Credit	0.12	No feature noise or label bias	
	0.23	No feature noise and 30% label bias	
	0.3	feature noise $\sim N(0.5, 0.5)$ and 45% label bias	
	0.4	feature noise $\sim N(1, 0.5)$ and 45% label bias	
Weather	0.11	Tropical, Mild temperate	
	0.19	Tropical, Mild temperate	Dry, Mild temperate
	0.30	Tropical, Mild temperate	Dry
	0.40	Tropical, Mild temperate	Dry, Snow
	0.48	Tropical, Mild temperate	Snow
EMNIST	0.11	1-10	
	0.19	1-10, 12,18,24,28	1-10, 38,44,50,54
	0.25	1-10, 11,12,13,14,16,18,24,28	1-10, 37,38,39,40,42,44,50,54
	0.34	1-10, 11-25	1-10, 36-41
	0.39	1-10, 11-35	1-10, 36-61
CIFAR	0.08	1-10	
	0.21	11,98,29,73, 78, 49, 97, 51, 55, 92	11,98,29,73, 78, 49, 42, 83, 72, 82
	0.30	11,50,78,1,92, 78, 49, 97, 55, 16, 14	11, 36, 29, 73, 82, 78, 49, 42, 12, 23, 51
	0.38	11,50,78,8,92,2,49,98,89,3	17, 36, 30, 73, 83,28, 34, 42, 10, 20
IXITiny	0.08	Guys	Hammersmith
	0.28	Guys	IOP
	0.30	Hammersmith	IOP
ISIC2019	0.06	ViDIR Group, Vienna (FOTO)	ViDIR Group, Vienna (FOTO)
	0.15	ViDIR Group, Vienna (FOTO)	Hospital Clínic de Barcelona
	0.19	ViDIR Group, Vienna (FOTO)	ViDIR Group, Vienna (Dermaphot)
	0.25	ViDIR Group, Vienna (FOTO)	ViDIR Group, Vienna (MoleMax)
	0.3	ViDIR Group, Vienna (MoleMax)	Cliff Rosendahl, Australia

Table D.1: Creation of partitioned datasets

* Note these examples are not assessed during model training and are for illustrative purposes only.

algorithms. For pFedME we use the pFedME optimizer released by the authors. For CIFAR, IXITiny and ISIC2019 we utilize pre-trained models that we fine-tune. Below we describe the model, learning rates, optimizers, and regularization parameters (for pFedME and Ditto only) for each dataset.

Synthetic We use a MLP with 2 hidden layers of size 18 and 6.

Table D.2:

OT score	Single	Joint	FedAvg	pFedME	Ditto
0.03	$5e^{-3}$, ADM	$5e^{-2}$, ADM	$5e^{-2}$, ADM	$5e^{-2}$, pFedME-opt, $5e^{-1}$	$1e^{-1}$, ADM, $5e^{-1}$
0.10	$5e^{-3}$, ADM	$5e^{-2}$, ADM	$1e^{-1}$, ADM	$1e^{-1}$, pFedME-opt, $5e^{-1}$	$1e^{-1}$, ADM, $1e^0$
0.20	$1e^{-2}$, ADM	$1e^{-1}$, ADM	$1e^{-1}$, ADM	$1e^{-1}$, pFedME-opt, $1e^{-1}$	$1e^{-1}$, ADM, $1e^{-1}$
0.30	$5e^{-2}$, ADM	$5e^{-3}$, ADM	$5e^{-2}$, SGD	$5e^{-2}$, pFedME-opt, $1e^{-2}$	$1e^{-1}$, SGD, $1e^{-2}$
0.40	$5e^{-2}$, ADM	$1e^{-2}$, ADM	$5e^{-2}$, SGD	$5e^{-2}$, pFedME-opt, $1e^{-2}$	$1e^{-1}$, SGD, $1e^{-2}$
0.50	$5e^{-2}$, ADM	$3e^{-2}$, ADM	$5e^{-2}$, SGD	$1e^{-1}$, pFedME-opt, $1e^{-3}$	$1e^{-1}$, SGD, $1e^{-3}$

Credit We use a MLP with 3 hidden layers of size 56, 56 and 28.

Table D.3:

OT score	Single	Joint	FedAvg	pFedME	Ditto
0.12	$5e^{-3}$, ADM	$5e^{-2}$, ADM	$5e^{-2}$, ADM	$1e^{-1}$, pFedME-opt, $5e^{-1}$	$1e^{-1}$, ADM, $1e^0$
0.23	$5e^{-3}$, ADM	$1e^{-2}$, ADM	$1e^{-2}$, ADM	$1e^{-1}$, pFedME-opt, $1e^{-1}$	$1e^{-1}$, ADM, $1e^{-1}$
0.30	$1e^{-2}$, ADM	$1e^{-2}$, ADM	$1e^{-2}$, ADM	$1e^{-1}$, pFedME-opt, $1e^{-2}$	$1e^{-1}$, ADM, $1e^{-3}$
0.40	$5e^{-2}$, ADM	$1e^{-3}$, ADM	$5e^{-3}$, ADM	$1e^{-1}$, pFedME-opt, $1e^{-2}$	$1e^{-1}$, ADM, $1e^{-3}$

Weather We use a MLP with 3 hidden layers of size 123, 123 and 50.

Table D.4:

OT score	Single	Joint	FedAvg	pFedME	Ditto
0.11	$3e^{-3}$, ADM	$1e^{-2}$, ADM	$5e^{-2}$, SGD	$1e^{-1}$, pFedME-opt, $5e^{-1}$	$1e^{-1}$, ADM, $1e^0$
0.19	$5e^{-3}$, ADM	$5e^{-2}$, ADM	$1e^{-1}$, SGD	$1e^{-1}$, pFedME-opt, $5e^{-1}$	$1e^{-1}$, ADM, $1e^0$
0.30	$1e^{-2}$, ADM	$1e^{-2}$, ADM	$5e^{-2}$, SGD	$1e^{-1}$, pFedME-opt, $1e^{-1}$	$1e^{-1}$, ADM, $5e^{-1}$
0.40	$1e^{-2}$, ADM	$1e^{-3}$, ADM	$2e^{-2}$, SGD	$1e^{-1}$, pFedME-opt, $1e^{-2}$	$1e^{-1}$, ADM, $1e^{-2}$
0.48	$1e^{-2}$, ADM	$1e^{-3}$, ADM	$5e^{-2}$, SGD	$1e^{-1}$, pFedME-opt, $1e^{-3}$	$1e^{-1}$, ADM, $1e^{-2}$

EMNIST We use a LeNet-5 CNN.

Table D.5:

OT score	Single	Joint	FedAvg	pFedME	Ditto
0.11	$5e^{-2}$, ADM	$1e^{-2}$, ADM	$5e^{-2}$, ADM	$5e^{-2}$, pFedME-opt, $1e^{-1}$	$5e^{-2}$, ADM, $5e^{-1}$
0.19	$5e^{-3}$, ADM	$5e^{-3}$, ADM	$5e^{-2}$, ADM	$5e^{-2}$, pFedME-opt, $1e^{-1}$	$5e^{-2}$, ADM, $1e^{-1}$
0.25	$1e^{-2}$, ADM	$5e^{-3}$, ADM	$5e^{-2}$, ADM	$5e^{-2}$, pFedME-opt, $1e^{-2}$	$1e^{-1}$, ADM, $1e^{-2}$
0.34	$1e^{-2}$, ADM	$1e^{-2}$, ADM	$1e^{-2}$, ADM	$5e^{-2}$, pFedME-opt, $1e^{-2}$	$1e^{-1}$, ADM, $1e^{-3}$
0.39	$1e^{-2}$, ADM	$5e^{-3}$, ADM	$3e^{-2}$, ADM	$1e^{-1}$, pFedME-opt, $1e^{-3}$	$5e^{-2}$, ADM, $1e^{-3}$

CIFAR We use a pre-trained ResNet-18, freezing layers 1-3.

Table D.6:

OT score	Single	Joint	FedAvg	pFedME	Ditto
0.08	$1e^{-3}$, ADM	$5e^{-4}$, ADM	$1e^{-2}$, ADM	$1e^{-2}$, pFedME-opt, $5e^{-1}$	$5e^{-3}$, ADM, $1e^0$
0.21	$1e^{-3}$, ADM	$5e^{-3}$, ADM	$1e^{-2}$, SGD	$5e^{-2}$, pFedME-opt, $1e^{-1}$	$1e^{-2}$, ADM, $5e^{-1}$
0.30	$5e^{-4}$, ADM	$5e^{-2}$, ADM	$1e^{-2}$, SGD	$5e^{-2}$, pFedME-opt, $1e^{-2}$	$1e^{-2}$, ADM, $1e^{-2}$
0.38	$5e^{-4}$, ADM	$5e^{-3}$, ADM	$5e^{-2}$, SGD	$5e^{-2}$, pFedME-opt, $1e^{-3}$	$5e^{-3}$, ADM, $1e^{-2}$

IXITiny We use a pre-trained 3D Unet and allow training of all layers.

Table D.7:

OT score	Single	Joint	FedAvg	pFedME	Ditto
0.08	$1e^{-1}$, ADM	$1e^{-1}$, ADM	$5e^{-2}$, ADM	$1e^{-1}$, pFedME-opt, $5e^{-1}$	$1e^{-1}$, ADM, $1e^{-1}$
0.28	$1e^{-1}$, ADM	$1e^{-1}$, ADM	$1e^{-1}$, SGD	$5e^{-2}$, pFedME-opt, $1e^{-2}$	$1e^{-1}$, SGD, $1e^{-2}$
0.30	$1e^{-1}$, ADM	$1e^{-2}$, ADM	$1e^{-1}$, SGD	$5e^{-2}$, pFedME-opt, $1e^{-3}$	$1e^{-3}$, SGD, $1e^{-2}$

ISIC2019 We use a pre-trained efficientNet and allow training of all layers.

Table D.8:

OT score	Single	Joint	FedAvg	pFedME	Ditto
0.06	$5e^{-4}$, ADM	$5e^{-3}$, ADM	$1e^{-1}$, ADM	$5e^{-3}$, pFedME-opt, $5e^{-1}$	$1e^{-2}$, ADM, $5e^{-1}$
0.15	$5e^{-3}$, ADM	$5e^{-3}$, ADM	$1e^{-2}$, ADM	$5e^{-3}$, pFedME-opt, $1e^{-1}$	$1e^{-1}$, ADM, $1e^{-1}$
0.19	$5e^{-3}$, ADM	$5e^{-3}$, ADM	$1e^{-2}$, ADM	$5e^{-3}$, pFedME-opt, $1e^{-1}$	$1e^{-1}$, ADM, $1e^{-1}$
0.25	$5e^{-3}$, ADM	$1e^{-2}$, ADM	$1e^{-2}$, ADM	$1e^{-2}$, pFedME-opt, $1e^{-2}$	$1e^{-2}$, ADM, $1e^{-2}$
0.3	$5e^{-3}$, ADM	$5e^{-3}$, ADM	$5e^{-2}$, ADM	$1e^{-2}$, pFedME-opt, $1e^{-3}$	$1e^{-2}$, ADM, $1e^{-2}$

*ADM = Adam optimizer, SGD = SGD optimizer, pFedME-opt = pFedME optimizer

D.2 Results: Estimates Using Privacy-preserving Calculations

Figure D.2 compares the calculated score from the plain-text algorithms and the privacy-preserving algorithms. We show that the MPC protocol introduces no error ($\leq 1e^{-6}$) when calculating feature costs and the z-CDP protocol introduces minimal error across most label comparisons.

D.3 Results: Synthetic Results for Costs > 0.5

Figure D.2 presents the results obtained from synthetic datasets with scores of 0.6, 0.8, and 1.0. To generate these datasets, we employed a combination of label switching and feature distributions that are deliberately contrasting. While such a scenario may not directly mirror real-world conditions, it helps with intuition of our score.

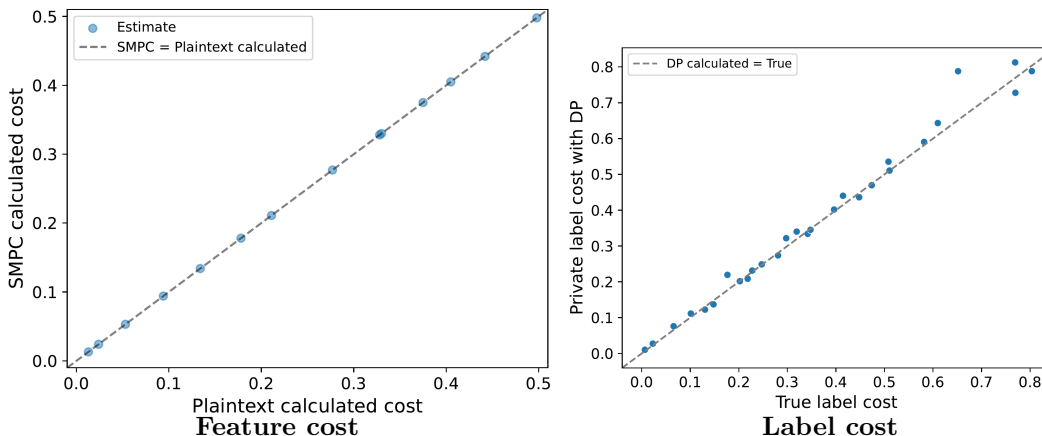


Figure D.1: Scores calculated in plaintext vs. privacy-preserving algorithm. Dashed $Y=X$ represents perfect agreement.

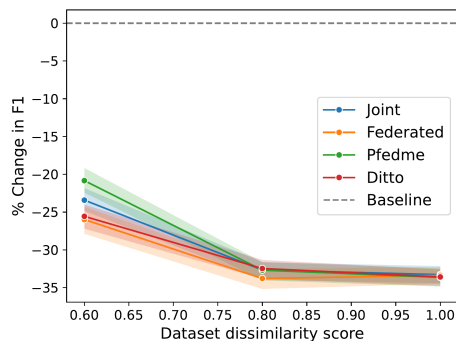


Figure D.2: Performance of models trained on Synthetic dataset with scores 0.6, 0.8, 1.0. Results expressed as percentage changes from single baseline with Joint (blue), Federated (orange), pFedME (green) and Ditto (Red)

D.4 Results: Weight Divergence Correlation

We assess the relationship between weight divergence and two metrics: our proposed metric and the original Wasserstein distance using Pearson correlation tests (Table D.4). Our findings indicate that our metric consistently exhibits a higher correlation across all datasets when compared to the original Wasserstein distance ($p= 0.012$).

Dataset	Our metric	Wasserstein
Synthetic	0.98	0.96
Credit	0.94	0.90
Weather	0.99	0.69
EMNIST	0.99	0.68
CIFAR	0.97	0.85
ISIC	0.89	0.88
IXITiny	0.97	0.83

Table D.9: Comparison of Pearson Correlation Coefficients: Weight Divergence vs. Our Metric and Wasserstein Distance Across All Datasets

D.5 Results: MPC Runtime Complexity

Dot product Using the protocol outline by Du et al. (2004), the runtime complexity of the dot product protocol is $O(n^2d + d^2)$. Here, n is the number of samples and d is the vector dimension. The $O(d^2)$ term arises from inversion of an MDS code matrix Jog (2004). The dominating term in the complexity depends on the relative size of sample count, n , to the dataset dimension, d .

Euclidean distance We also analyzed a protocol by Ravikumar et al. (2004) to calculate euclidean distance in MPC. We chose this protocol as it also does not require encryption making it computationally efficient. The protocol provides a probabilistic estimate of the euclidean distance based on the number of indices from each vector that is used in the secure intersection step of the protocol. If one desires an exact euclidean distance estimate, then all indices must be sampled and the complexity is $O(n^2(d + d\log(d)))$ where n is the number of samples and d is the vector dimension.

D.6 Results: Hyperparameters

In this section we present sensitivity analysis for hyperparameters.

D.6.1 Regularization Parameter ϵ

We conducted sensitivity analysis on the regularization parameter ϵ evaluating results obtained from $5e^{-3}$, $1e^{-2}$, $5e^{-2}$, $1e^{-1}$, $5e^{-1}$, 1, 10, 100, 1000, 10000, compared to the baseline $\epsilon = 1e^{-3}$. Our findings indicate that at values below $5e^{-2}$ the results are largely consistent (Figure D.3).

D.6.2 Feature-to-label Ratio (λ)

We conduct a sensitivity analysis on the feature-to-cost label ratio. Our baseline, 2:1, arises from the fact that cosine similarity and Hellinger distance range from 0-2 and 0-1, respectively. We compare ratios: 1:1, 1:2, 1:3, 1:4, 1:5, 3:1, 4:1, 5:1. Our results show that the score is robust to a range of ratios within the 1:4-4:1 (Figure D.4).

DATASET SIMILARITY FOR FL

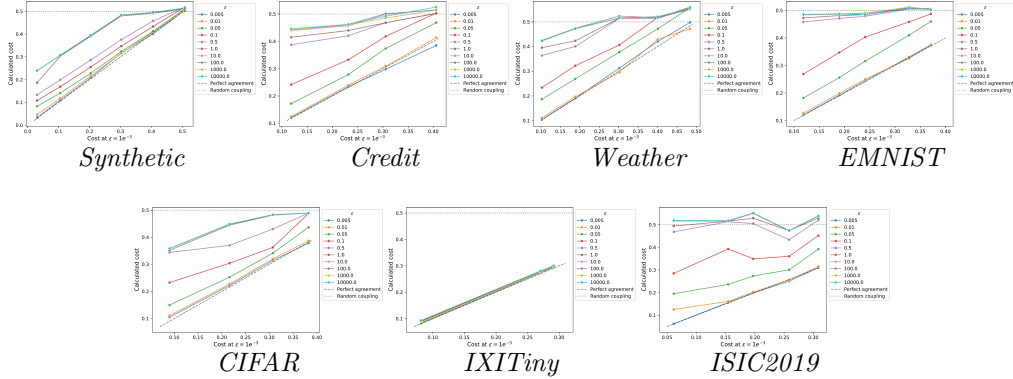


Figure D.3: Scores calculated at varying ϵ values vs. scores calculated at $\epsilon = 1e^{-3}$. Dashed $Y=X$ represents perfect agreement with $\epsilon = 1e^{-3}$

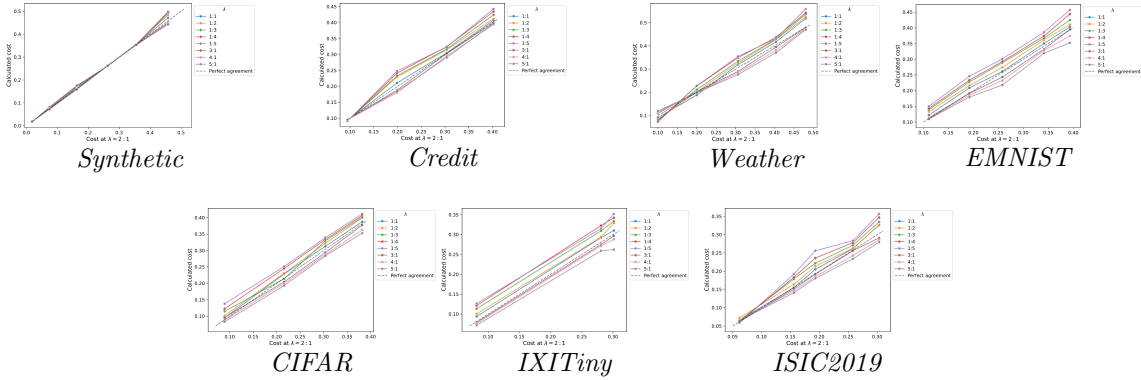


Figure D.4: Scores calculated at varying feature-to-label cost ratios. Dashed $Y=X$ represents perfect agreement with 2:1 ratio.

Appendix E. Privacy Guarantees

This section covers the analysis for the combined application of MPC and z-CDP to calculate feature and label costs, respectively.

Setup

Let sites 1 and 2 hold datasets $X \in \mathbb{R}^{n \times d}$ and $Y \in \mathbb{R}^{n \times d}$ where n is the number of samples and d is the dataset dimension, respectively. All samples in X and Y belong to a specific label class $c \in C$ where $C = \{c_1, \dots, c_l\}$. We use X_c and Y_c to denote the samples in X and Y that belong to label class c . Algorithm 1 releases the following information to the server:

1. XY^T , the cosine similarity matrix calculated using MPC (Section B.2)

2. $\mu_{X'_c}$ and $\mu_{Y'_c}, \forall c \in C$, the noised column means of X_c and Y_c such that $\mu_{X'_c} = \mu_{X_c} + e_1$ and $\mu_{Y'_c} = \mu_{Y_c} + e_2$ where e_1, e_2 are noise vectors generated using a ρ -zCDP mechanism.
3. $X'_c{}^T X'_c$ and $Y'_c{}^T Y'_c, \forall c \in C$, the noised covariance matrices of X_c and Y_c such that $X'_c{}^T X'_c = X_c^T X_c + E_1$ and $Y'_c{}^T Y'_c = Y_c^T Y_c + E_2$ where E_1, E_2 are symmetric noise matrices generated using a ρ -zCDP mechanism.

Threat Model

In our threat model we assume the adversary has access to all released information ($XY^T, \mu_{X'_c}, \mu_{Y'_c}, X'_c{}^T X'_c, Y'_c{}^T Y'_c$) and aims to reconstruct X or Y .

Assumptions

We make the following assumptions on X and Y :

- All samples in X and Y are independent.
- All samples in X and Y belong to one class such that $X_c = X$ and $Y_c = Y$. Consequently, the summary statistics of the full datasets are released. This represents a *worst-case* scenario.
- X and Y are column-centered and row-normalized independently. This pre-processing is a requirement of Algorithm 1. This has the following implications:
 1. Row-normalization ensures that each entry x_{ij} of X satisfies $|x_{ij}| \leq 1$.
 2. As a consequence of 1, the entries of XX^T are bounded by -1 and 1, with the diagonal entries being 1.
 3. As a consequence of 1, the diagonal entries of $X^T X$, which represent the variance of the features, is at most $\frac{1}{3}$. This arises under a uniform distribution with values x_{ij} between -1 and 1.
 4. Column centering prior to calculating $\mu_{X'}$ and $\mu_{Y'}$ ensures that $\mu_{X'}$ and $\mu_{Y'}$ do not release information.

E.0.3 Proof Outline

Assuming that an adversary has access to $X'^T X', Y'^T Y'$ and XY^T , our goal is to determine what information regarding datasets X or Y can be leaked. Without loss of generality, we focus on X . To quantify the leakage, we bound the ability of an adversary to reconstruct X using $X'^T X'$ and XY^T . In summary, an adversary can reconstruct X up to an orthonormal basis if the singular vectors of $X'^T X'$ and XY^T are sufficiently close to $X^T X$ and XX^T , respectively. In the proof, **we bound how closely the singular vectors of $X'^T X'$ and XY^T can approximate the singular vectors of $X^T X$ and XX^T .**

The proof relies on matrix perturbation theory framing $X'^T X'$ and XY^T as perturbed versions of $X^T X$ and XX^T . Under this framework, the singular vectors of $X'^T X'$ and XY^T matrix can only approximate $X^T X$ and XX^T when the spectral gap of $X^T X$ and XX^T , $\delta := \sigma_1 - \sigma_2$ is larger than the spectral norm of the perturbation (Vu, 2011). We show that,

under some assumptions and constraints on the data, the perturbation is larger than the upper bound of the spectral gaps in both $X'^T X'$ and XY^T .

Preliminaries

We use the following preliminaries:

1. **Singular value decomposition (SVD):**

- The SVD of X is expressed as $X = U_X \Sigma_X V_X$ which are the left singular vectors, singular values, and right singular vectors, respectively.
- The SVD decomposition of XX^T yields U_X and Σ_X and the SVD decomposition of $X^T X$ yields V_X and Σ_X .
- With U_X , Σ_X , and V_X it is possible to reconstruct X up to an orthonormal basis.

2. **Matrix trace:** The trace of a matrix A is the sum of the diagonal elements, $tr(A) = \sum_{i=1}^n a_{i,i}$. The trace is also sum of the eigenvalues, σ , of A , $tr(A) = \sum_{i=1}^n \sigma_i$.

3. **Norms:**

- The Frobenius norm of matrix A is $\|A\|_F = \sqrt{\sum_{i=1}^n \sum_{j=1}^n a_{ij}^2}$
- The spectral norm of a matrix, $\|\cdot\|$, is the maximum singular value of the matrix, $\max\{\sigma_i\}_{i=1}^n$ for a matrix with singular values $\sigma_1, \dots, \sigma_n$
- The spectral norm is upper bounded by the Frobenius norm, $\|\cdot\| \leq \|\cdot\|_F$

4. **Spectral norm of random matrix:** Let E be a random symmetric matrix in $\mathbb{R}^{d \times d}$ where each entry $e_i \sim N(0, \sigma)$ then:

$$2\sigma\sqrt{d} - c \ln d \geq \|E\| \leq 2\sigma\sqrt{d} + cd^{\frac{1}{4}} \ln d$$

for some constant c . As $n \rightarrow \infty$ then $\|E\|$ is expected to be at least $2\sigma\sqrt{n}$ Vu (2005).

5. **Spectral gap:** The spectral gap of a matrix, δ_i , is defined as $\delta_i := \sigma_i - \sigma_{i+1}$ where σ_i is the i^{th} singular value.
6. **Wedin Sin theorem:** This theorem provides a bound on how closely the singular vectors of a perturbed matrix, A' approximates the singular vectors of the original matrix, A

$$\sin\Theta(V_A, V_{A'}) \leq C \frac{\|E\|}{\delta}$$

where δ is the first spectral gap, $V_A, V_{A'}$ are the singular vectors, $\|E\|$ is the spectral norm of the perturbation matrix E and C is a constant > 0 . If $\delta \geq C\|E\|$ then:

$$\sin\Theta(V_A, V_{A'}) \leq \epsilon.$$

However, if $\delta < C\|E\|$ then it no longer holds that $V_{A'}$ closely approximates V_A (Vu, 2011).

7. **Jensen's inequality:** Jensen's inequality for a convex function $f(\cdot)$ states

$$f\left(\frac{1}{n} \sum_{i=1}^n x_i\right) \leq \frac{1}{n} \sum_{i=1}^n f(x_i).$$

LEMMA 1: THE SPECTRAL GAPS OF XX^T AND $X^T X$ ARE n AND $\frac{d}{3}$, RESPECTIVELY

Let $XX^T \in \mathbb{R}^{n \times n}$ and $X^T X \in \mathbb{R}^{d \times d}$ where n and d are the number of samples and features, respectively. This proof relies on showing that the spectral gaps of XX^T and $X^T X$, δ_{XX^T} and $\delta_{X^T X}$ are less than the spectral norms of the perturbations. To do this, we first establish upper bounds on δ_{XX^T} and $\delta_{X^T X}$, leveraging the fact that both XX^T and $X^T X$ are symmetric matrices and X is row-normalized. In the case of XX^T , the bound is

$$\delta_{XX^T} < n.$$

The upper bound arises as $\sum_{i=1}^n \sigma_i = \text{tr}(XX^T)$, and under the assumption that all of this is concentrated on σ_1 with $\sigma_2 \rightarrow 0$. Since the diagonal entries of XX^T are all one (due to row-normalization), $\text{tr}(XX^T) = n$.

For $X^T X$, $\delta_{X^T X}$ is bounded as

$$\delta_{X^T X} < \frac{d}{3}.$$

This upper bound is derived from the fact that the diagonal entries of $X^T X$, which represent the variance of the features, are $\leq \frac{1}{3}$ (see Section D.6.2) and all of this concentrated in σ_1 . Consequently, $\text{tr}(X^T X) = \frac{d}{3}$. Note, these are upper bounds the gap is likely lower in real-world datasets with low intrinsic rank Vu (2011).

PROOF 1: BOUNDING THE INFORMATION FROM RELEASING $X'^T X'$

Next, we bound how closely the $V_{X'^T X'}$ approximates $V_{X^T X}$. Let E be the perturbation matrix where each entry $e_i \sim N(0, \frac{\Delta^2}{2\rho^2})$ and $\Delta = \frac{\sqrt{2}}{n} \left(d + 2\sqrt{d \log(n/\beta_s)} + 2\log(n/\beta_s) \right)$ where ρ and β_s are user defined parameters based on the privacy-budget (we set $\beta = 0.01, \rho = 0.1$). We can set a lower bound for Δ and σ as $\Delta \geq \frac{\sqrt{2}d}{n}$ and $\sigma \geq \frac{d}{\rho n}$. Using the result for a spectral norm of a random matrix, E , we get

$$\|E\| \geq \frac{2d^{\frac{3}{2}}}{\rho n}.$$

Thus, as long as the privacy parameters are appropriately set, then $\|E\| > \delta_{X^T X} = \frac{d}{3}$. Specifically, the bound on the privacy parameters is

$$\frac{6d^{\frac{1}{2}}}{n} > \rho,$$

then $\|E\| > \delta_{X^T X}$. Appropriately setting ρ should ensure sufficient protection. Across all our datasets, $\rho = 0.1$ met this criterion but this will vary depending on the specific datasets.

PROOF 2: BOUNDING THE INFORMATION FROM RELEASING XY^T

Next, we bound how closely the V_{XY^T} approximates V_{XX^T} . To do this, we quantify how much X and Y must differ such that XY^T does not reveal U_{XX^T} . This is an argument on the overlap in samples of X and Y . For example, in an extreme case, if all samples overlap then $XX^T = XY^T$ and U_{XX^T} is perfectly approximated by U_{XY^T} . To estimate the minimum difference, we leverage the fact that XX^T and XY^T are bounded $-1, 1$. We define

the perturbation matrix $P = XY^T - XX^T$. When samples in X and Y overlap, entries in P will be 0, otherwise entries will be non-zero. We can bound spectral norm of P using the Frobenius norm of P by using the fact that $\|P\| \leq \|P\|_F$ and $\|P\|_F$ is itself bounded as all entries in XY^T are between -1,1

$$0 \leq \|P\| \leq \|P\|_F \leq 2n.$$

The lower bound arises when XY^T and XX^T are identical and the upper bound occurs when every XY^T and XX^T maximally differ and entries $p_{ij} = -2$ or 2 . To obtain how much X and Y can differ for $\|P\| > \delta_{XX^T} = n$, we derive a bound on $\|P\|_F$. Let $\alpha_F = \frac{1}{n(n-1)} \sum p_{ij}^2$ such that α_F represents the average squared contribution of p_{ij} to $\|P\|_F$. Let $\alpha = \left(\frac{1}{n(n-1)} \sum p_{ij}\right)^2$ such that α represents the mean entry of P squared. As entries in P are between -2,2, α ranges from 0,4. We are actually interested in α_F but invoke Jensen’s inequality to lower bound α_F by α . In this case, a threshold is needed such that XY^T does not reveal U_{XX^T} . This threshold is

$$\sqrt{\alpha_F}n \geq \sqrt{\alpha}n > n.$$

It is clear that α must be ≥ 1 for $\|P\| > \delta_{XX^T}$. As α ranges from 0,4 (as entries in P , or $\sqrt{\alpha}$, range from -2,2), a requirement of $\alpha \geq 1$ suggests Y must differ by at least a 25% difference in entries between XY^T and XX^T . Note, this bound assumes $\delta_{XY^T} = n$ which is conservative. In reality, δ_{XY^T} is smaller and α can be less than 1.

Limitations

We assume worse-case spectral gaps of XX^T and $X^T X$. A tighter bound on the spectral gaps would *reduce the level noise added to $X'^T X'$ and the necessary deviation between XX^T and XY^T* to prevent reconstruction. We have not pursued these tighter bounds as they are dataset specific. Further, we do not consider repeated release of different matrices (e.g., repeated release with different differential privacy noise) as our setting differs from querying databases. XY^T and $X'^T X'$ are released only once in our scenario.

Conclusion

We have demonstrated that the release of $X'^T X'$ and XY^T will not allow for the reconstruction of X .

References

Alessandro Achille, Glen Mbeng, and Stefano Soatto. Dynamics and reachability of learning tasks. *arXiv preprint arXiv:1810.02440*, 2018.

Alessandro Achille, Michael Lam, Rahul Tewari, Avinash Ravichandran, Subhansu Maji, Charless C Fowlkes, Stefano Soatto, and Pietro Perona. Task2vec: Task embedding for meta-learning. In *Proceedings of the IEEE/CVF international conference on computer vision*, pages 6430–6439, 2019.

David Alvarez-Melis and Nicolo Fusi. Geometric dataset distances via optimal transport. *Advances in Neural Information Processing Systems*, 33:21428–21439, 2020.

- David Alvarez-Melis and Nicolò Fusi. Dataset dynamics via gradient flows in probability space. In *International Conference on Machine Learning*, pages 219–230. PMLR, 2021.
- Mahsa Baktashmotlagh, Mehrtash T Harandi, Brian C Lovell, and Mathieu Salzmann. Domain adaptation on the statistical manifold. In *Proceedings of the IEEE conference on computer vision and pattern recognition*, pages 2481–2488, 2014.
- Shai Ben-David, John Blitzer, Koby Crammer, and Fernando Pereira. Analysis of representations for domain adaptation. *Advances in neural information processing systems*, 19, 2006.
- Jeremiah Birrell, Paul Dupuis, Markos A Katsoulakis, Yannis Pantazis, and Luc Rey-Bellet. (f, γ) -divergences: interpolating between f -divergences and integral probability metrics. *The Journal of Machine Learning Research*, 23(1):1816–1885, 2022.
- Sourav Biswas, Yihe Dong, Gautam Kamath, and Jonathan Ullman. Coinpress: Practical private mean and covariance estimation. *Advances in Neural Information Processing Systems*, 33:14475–14485, 2020.
- Brain-development.org. Ixi dataset. URL brain-development.org/ixi-dataset/. Accessed: 2023-09-18.
- Mark Bun and Thomas Steinke. Concentrated differential privacy: Simplifications, extensions, and lower bounds. In *Theory of Cryptography Conference*, pages 635–658. Springer, 2016.
- Declan Butler. Data sharing threatens privacy. *Nature*, 449(7163):644–645, October 2007.
- Sentao Chen, Lin Zheng, and Hanrui Wu. Riemannian representation learning for multi-source domain adaptation. *Pattern Recognition*, 137:109271, 2023.
- David A Cieslak, T Ryan Hoens, Nitesh V Chawla, and W Philip Kegelmeyer. Hellinger distance decision trees are robust and skew-insensitive. *Data Mining and Knowledge Discovery*, 24:136–158, 2012.
- Corinna Cortes and Mehryar Mohri. Domain adaptation in regression. In *International Conference on Algorithmic Learning Theory*, pages 308–323. Springer, 2011.
- Nicolas Courty, Rémi Flamary, Amaury Habrard, and Alain Rakotomamonjy. Joint distribution optimal transportation for domain adaptation. *Advances in neural information processing systems*, 30, 2017.
- Marco Cuturi. Sinkhorn distances: Lightspeed computation of optimal transport. *Advances in neural information processing systems*, 26, 2013.
- Bharath Bhushan Damodaran, Benjamin Kellenberger, Rémi Flamary, Devis Tuia, and Nicolas Courty. Deepjdot: Deep joint distribution optimal transport for unsupervised domain adaptation. In *Proceedings of the European conference on computer vision (ECCV)*, pages 447–463, 2018.

- Ittai Dayan, Holger R Roth, Aoxiao Zhong, Ahmed Harouni, Amilcare Gentili, Anas Z Abidin, Andrew Liu, Anthony Beardsworth Costa, Bradford J Wood, Chien-Sung Tsai, et al. Federated learning for predicting clinical outcomes in patients with covid-19. *Nature medicine*, 27(10):1735–1743, 2021.
- Wenliang Du, Yunghsiang S Han, and Shigang Chen. Privacy-preserving multivariate statistical analysis: Linear regression and classification. In *Proceedings of the 2004 SIAM international conference on data mining*, pages 222–233. SIAM, 2004.
- Cynthia Dwork and Guy N Rothblum. Concentrated differential privacy. *arXiv preprint arXiv:1603.01887*, 2016.
- Cynthia Dwork, Aaron Roth, et al. The algorithmic foundations of differential privacy. *Foundations and Trends® in Theoretical Computer Science*, 9(3–4):211–407, 2014.
- David Evans, Vladimir Kolesnikov, and Mike Rosulek. A pragmatic introduction to secure Multi-Party computation, 2018.
- Joseph Futoma, Morgan Simons, Trishan Panch, Finale Doshi-Velez, and Leo Anthony Celi. The myth of generalisability in clinical research and machine learning in health care. *The Lancet Digital Health*, 2(9):e489–e492, 2020.
- Matthias Gelbrich. On a formula for the l2 wasserstein metric between measures on euclidean and hilbert spaces. *Mathematische Nachrichten*, 147(1):185–203, 1990.
- Aude Genevay, Lénaïc Chizat, Francis Bach, Marco Cuturi, and Gabriel Peyré. Sample complexity of sinkhorn divergences. In *The 22nd international conference on artificial intelligence and statistics*, pages 1574–1583. PMLR, 2019.
- Víctor González-Castro, Rocío Alaiz-Rodríguez, and Enrique Alegre. Class distribution estimation based on the hellinger distance. *Information Sciences*, 218:146–164, 2013.
- Andreas Grammenos, Rodrigo Mendoza Smith, Jon Crowcroft, and Cecilia Mascolo. Federated principal component analysis. *Advances in Neural Information Processing Systems*, 33:6453–6464, 2020.
- Kaiming He, Xiangyu Zhang, Shaoqing Ren, and Jian Sun. Delving deep into rectifiers: Surpassing human-level performance on imagenet classification. In *Proceedings of the IEEE international conference on computer vision*, pages 1026–1034, 2015.
- Jeff Heaton. Ian goodfellow, yoshua bengio, and aaron courville: Deep learning: The mit press, 2016, 800 pp, isbn: 0262035618. *Genetic programming and evolvable machines*, 19(1-2):305–307, 2018.
- George Hripcsak and David J Albers. Next-generation phenotyping of electronic health records. *Journal of the American Medical Informatics Association*, 20(1):117–121, 2013.
- Kevin Hsieh, Amar Phanishayee, Onur Mutlu, and Phillip Gibbons. The non-iid data quagmire of decentralized machine learning. In *International Conference on Machine Learning*, pages 4387–4398. PMLR, 2020.

- Yutao Huang, Lingyang Chu, Zirui Zhou, Lanjun Wang, Jiangchuan Liu, Jian Pei, and Yong Zhang. Personalized cross-silo federated learning on non-iid data. In *Proceedings of the AAAI conference on artificial intelligence*, volume 35, pages 7865–7873, 2021.
- CS Jog. The accurate inversion of vandermonde matrices. *Computers & Mathematics with Applications*, 47(6-7):921–929, 2004.
- Leonid V Kantorovich. Mathematical methods of organizing and planning production. *Management science*, 6(4):366–422, 1960.
- Michel Ledoux. *The concentration of measure phenomenon*. Number 89. American Mathematical Soc., 2001.
- Ling Li. *Data complexity in machine learning and novel classification algorithms*. California Institute of Technology, 2006.
- Qinbin Li, Yiqun Diao, Quan Chen, and Bingsheng He. Federated learning on non-iid data silos: An experimental study. In *2022 IEEE 38th International Conference on Data Engineering (ICDE)*, pages 965–978. IEEE, 2022.
- Tian Li, Shengyuan Hu, Ahmad Beirami, and Virginia Smith. Ditto: Fair and robust federated learning through personalization. In *International Conference on Machine Learning*, pages 6357–6368. PMLR, 2021.
- Tengyuan Liang, Tomaso Poggio, Alexander Rakhlin, and James Stokes. Fisher-rao metric, geometry, and complexity of neural networks. In *The 22nd international conference on artificial intelligence and statistics*, pages 888–896. PMLR, 2019.
- Bruce G Lindsay. Efficiency versus robustness: the case for minimum hellinger distance and related methods. *The annals of statistics*, 22(2):1081–1114, 1994.
- Weiyang Liu, Yandong Wen, Zhiding Yu, Ming Li, Bhiksha Raj, and Le Song. Sphreface: Deep hypersphere embedding for face recognition. In *Proceedings of the IEEE conference on computer vision and pattern recognition*, pages 212–220, 2017.
- Chunjie Luo, Jianfeng Zhan, Xiaohe Xue, Lei Wang, Rui Ren, and Qiang Yang. Cosine normalization: Using cosine similarity instead of dot product in neural networks. In *International Conference on Artificial Neural Networks*, pages 382–391. Springer, 2018.
- F J MacWilliams. *The Theory of Error-correcting Codes. Pt. 1*. 1977.
- Andrey Malinin, Andreas Athanopoulos, Muhamed Barakovic, Meritxell Bach Cuadra, Mark JF Gales, Cristina Granziera, Mara Graziani, Nikolay Kartashev, Konstantinos Kyriakopoulos, Po-Jui Lu, et al. Shifts 2.0: Extending the dataset of real distributional shifts. *arXiv preprint arXiv:2206.15407*, 2022.
- Yishay Mansour, Mehryar Mohri, and Afshin Rostamizadeh. Domain adaptation: Learning bounds and algorithms. *arXiv preprint arXiv:0902.3430*, 2009.

- Brendan McMahan, Eider Moore, Daniel Ramage, Seth Hampson, and Blaise Aguera y Arcas. Communication-efficient learning of deep networks from decentralized data. In *Artificial intelligence and statistics*, pages 1273–1282. PMLR, 2017.
- Gonzalo Mena and Jonathan Niles-Weed. Statistical bounds for entropic optimal transport: sample complexity and the central limit theorem. *Advances in neural information processing systems*, 32, 2019.
- Joseph P Near and Chiké Abuah. Programming differential privacy. URL: <https://wvm>, 2021.
- NIST. Differential privacy: The future of work and open challenges. <https://www.nist.gov/blogs/cybersecurity-insights/differential-privacy-future-work-open-challenges>, 2022. Accessed: 2023-04-11.
- Jean Ogier du Terrail, Samy-Safwan Ayed, Edwige Cyffers, Felix Grimberg, Chaoyang He, Regis Loeb, Paul Mangold, Tanguy Marchand, Othmane Marfoq, Erum Mushtaq, et al. Flamby: Datasets and benchmarks for cross-silo federated learning in realistic healthcare settings. *Advances in Neural Information Processing Systems*, 35:5315–5334, 2022.
- Michal Pándy, Andrea Agostinelli, Jasper Uijlings, Vittorio Ferrari, and Thomas Mensink. Transferability estimation using bhattacharyya class separability. In *Proceedings of the IEEE/CVF Conference on Computer Vision and Pattern Recognition*, pages 9172–9182, 2022.
- Fernando Pérez-García, Rachel Sparks, and Sébastien Ourselin. Torchio: a python library for efficient loading, preprocessing, augmentation and patch-based sampling of medical images in deep learning. *Computer Methods and Programs in Biomedicine*, 208:106236, 2021.
- Pradeep Ravikumar, William W Cohen, and Stephen E Fienberg. A secure protocol for computing string distance metrics. *PSDM held at ICDM*, pages 40–46, 2004.
- Mohamed El Amine Seddik, Cosme Louart, Mohamed Tamaazousti, and Romain Couillet. Random matrix theory proves that deep learning representations of gan-data behave as gaussian mixtures. In *International Conference on Machine Learning*, pages 8573–8582. PMLR, 2020.
- Canh T Dinh, Nguyen Tran, and Josh Nguyen. Personalized federated learning with moreau envelopes. *Advances in Neural Information Processing Systems*, 33:21394–21405, 2020.
- Xuezheng Tu, Kun Zhu, Nguyen Cong Luong, Dusit Niyato, Yang Zhang, and Juan Li. Incentive mechanisms for federated learning: From economic and game theoretic perspective. *IEEE transactions on cognitive communications and networking*, 8(3):1566–1593, 2022.
- Cédric Villani et al. *Optimal transport: old and new*, volume 338. Springer, 2009.
- Van Vu. Singular vectors under random perturbation. *Random Structures & Algorithms*, 39(4):526–538, 2011.

- Van H Vu. Spectral norm of random matrices. In *Proceedings of the thirty-seventh annual ACM symposium on Theory of computing*, pages 423–430, 2005.
- David Wen, Saad M Khan, Antonio Ji Xu, Hussein Ibrahim, Luke Smith, Jose Caballero, Luis Zepeda, Carlos de Blas Perez, Alastair K Denniston, Xiaoxuan Liu, et al. Characteristics of publicly available skin cancer image datasets: a systematic review. *The Lancet Digital Health*, 4(1):e64–e74, 2022.
- Jason Yosinski, Jeff Clune, Anh Nguyen, Thomas Fuchs, and Hod Lipson. Understanding neural networks through deep visualization. *arXiv preprint arXiv:1506.06579*, 2015.
- Matthew D Zeiler and Rob Fergus. Visualizing and understanding convolutional networks. In *Computer Vision–ECCV 2014: 13th European Conference, Zurich, Switzerland, September 6–12, 2014, Proceedings, Part I 13*, pages 818–833. Springer, 2014.
- J. Zenn. Image-autoencoder. <https://github.com/jzenn/Image-AutoEncoder>, 2021.
- Angela Zhang, Lei Xing, James Zou, and Joseph C Wu. Shifting machine learning for healthcare from development to deployment and from models to data. *Nature Biomedical Engineering*, 6(12):1330–1345, 2022.
- Sicheng Zhao, Bo Li, Pengfei Xu, and Kurt Keutzer. Multi-source domain adaptation in the deep learning era: A systematic survey. *arXiv preprint arXiv:2002.12169*, 2020.
- Yue Zhao, Meng Li, Liangzhen Lai, Naveen Suda, Damon Civin, and Vikas Chandra. Federated learning with non-iid data. *arXiv preprint arXiv:1806.00582*, 2018.